POLITECNICO DI MILANO
School of Systems Engineering
MSc of Mathematical Engineering

Graduation thesis in Computational Sciences for Engineering

Numerical modeling of porosity evolution in source rock during kerogen breakdown

Advisors:

Prof. Luca Formaggia

Dr. Anna Scotti

Candidate:

Bianca Giovanardi

783039

Academic Year 2012-2013

Contents

List of Figures

Abstract

This thesis, carried out in collaboration with Eni S.p.A., aims at understanding how the porosity of the source rock, where hydrocarbons are generated, changes as generation and expulsion of hydrocarbons take place. In particular, the mechanical compaction, due to the effective stress, and the extra pore space generated by the consumption of the solid organic matter (i.e. kerogen) have a deep impact on the porosity of the rocks, as well as on the variations of pressure due to the breakdown of kerogen into fluid hydrocarbons and to the expulsion of these products. An original feature of this work is that the equations are formulated and numerically solved on a fixed domain, obtained from the physical one as its completely compacted configuration, having removed all the degradable part of the rock. The advantage is that the mesh can be built once and for all at the beginning of the simulation, as well as the basis functions of the finite element methods. Simulations are carried out in a two dimensional section of a sedimentary basin with a simplified model of source rock - which consists of rock with no hydrocarbon potential, pure kerogen, and a void part initially filled with water - and a simplified chemical kinetic, in which kerogen generates only oil. The temperature and the overburden due to the overlying sedimentary layers are given fields and may account for the burial history of the source rock, while the pressure of the fluids in place is modeled with the Darcy law.

Sommario

Le simulazioni numeriche nel campo dell'esplorazione petrolifera sono diventate uno strumento di routine che consente di supportare l'analisi geologica nella localizzazione degli idrocarburi dalla loro generazione nella roccia madre fino all'accumulo nel giacimento. Gli idrocarburi sono generati dalla decomposizione termica del kerogene, un solido organico di origine biologica contenuto nella roccia madre. Requisito fondamentale è che la roccia madre sia collocata a una certa profondità, cosicché possa raggiungere le elevate temperature che consentono l'avvio del processo di decomposizione del kerogene in composti petroliferi. Per effetto della compattazione dei sedimenti, causata dal progressivo sovraccarico, una volta generati, gli idrocarburi sono espulsi dalla roccia madre e ha luogo la *migrazione primaria*. Per *migrazione secondaria* si intende, invece, lo spostamento compiuto dagli idrocarburi fuori dalla roccia madre attraverso pori più ampi e rocce più permeabili. Recentemente, gli studi condotti al fine dello sfruttamento dei giacimenti non convenzionali hanno messo in luce l'importanza di considerare i processi di ritenzione nella roccia madre, come ad esempio l'adsorbimento all'interno dei nanopori della roccia. Per *adsorbimento* si intende il fenomeno chimico-fisico che consiste nell'accumulo di una o più sostanze fluide sulla superficie di un solido.

Lo scopo di questa tesi, svolta in collaborazione con Eni S.p.A., è quello di modellizzare e simulare i processi di generazione e migrazione primaria degli idrocarburi, ponendo un'attenzione particolare all'evoluzione della porosità in risposta alla mutua interazione tra i processi chimici e fisici che coinvolgono la roccia madre. Da una parte, infatti, la porosità risente dell'aumento del sovraccarico, causato dalla progressiva sedimentazione; dall'altra, la degradazione del materiale organico solido in idrocarburi liquidi o gassosi tende a generare una ulteriore porosità.

Per effetto del consumo del kerogene e della compattazione dei sedimenti, il dominio fisico del problema evolve nel tempo. Al fine di evitare le complicazioni numeriche che ne conseguono, le equazioni del modello sono state mappate e risolte su un dominio fisso, ottenuto compattando completamente il dominio fisico e rimuovendo da esso la porzione degradabile della roccia. Una volta risolte le equazioni su questo dominio, la soluzione è stata riportata nel dominio fisico, per una visualizzazione più intuitiva.

Una parte della tesi è stata svolta in stage presso Eni S.p.A ed è stata dedicata allo studio e alla comparazione di diversi modelli di ritenzione, integrati all'interno di simulazioni di generazione e migrazione primaria. Sebbene il modello proposto in questa tesi non tenga conto di processi di questo tipo, riteniamo che questo studio si rivelerà utile in una futura estensione del modello che implementi cinetiche chimiche più complesse. Una lunga appendice è, pertanto, dedicata a questa parte del lavoro.

1 Introduction

Numerical simulations have become a routine tool for petroleum exploration to simulate both the processes of generation and expulsion from source rock and those of migration and accumulation in reservoirs. Since oil exploration is a very expensive and risky operation, it is important to have a deep knowledge of the geological background of the areas that will be explored. The numerical simulation of generation and migration processes can support geological analysis in tracking hydrocarbons "from source to trap" and therefore reduce the risk in oil exploration. The main information that the oil industry expects to understand with the combined investigation of numerical simulations and geological analysis is where the reservoirs are located and what is the amount of oil and gas that they will be able to find and exploit.

The generation of hydrocarbons never happens in the accumulation reservoirs where they are discovered. Indeed, hydrocarbons are generated in a source rock, i.e. a layer of sediments rich in organic matter, called kerogen. Because of its progressive burial, the source rock experiences high temperatures and the chemical reactions that cause the breakdown of kerogen into oil take place. Hydrocarbons are then expelled from the source rock as a consequence of the sediment compaction and primary migration takes place. Once expelled from the source rock, the petroleum starts a secondary migration, driven by buoyancy. The migration of petroleum continues as long as it does not meet with a layer of low permeability, which forms a trap, where the hydrocarbons accumulate.

A realistic numerical simulation of generation and primary migration allows, given the thermal history of the basin and the physical characteristics of the source rock, such as porosity and organic matter content, to estimate the amount of hydrocarbons generated throughout hundreds of million years. Moreover, numerical simulations can provide information on the timing of expulsion. Finally, if a detailed description of chemical reactions and retention processes is provided, it is possible to forecast the chemical composition of the products and the fraction of gas versus oil expelled. In this sense, numerical simulations support and complete the reconstructions made by geologists.

Recently, the studies about the exploitation of unconventional sources have stressed the importance of taking into account, in the study and simulation of generation and primary migration, retention processes in the source rock, such as the solution of hydrocarbons into the organic matter or the trapping of molecules in nanometric pores (see [16] and [17]). These phenomena depend strongly on the molecular properties of the gas and oil species, therefore some types of hydrocarbons are more likely to be retained than others. Since retained hydrocarbons keep reacting and breaking into lighter compounds, retention processes can significantly alter the final chemical

composition of the products

This thesis aims at modeling and simulating the porosity evolution in the source rock, during the processes of generation and primary migration. In the source rocks a complex interplay of mechanical and chemical processes affects on the one hand the balance of the vertical stress, and on the other the kerogen concentration field. Both these effects have strong implications on porosity and, consequently, on permeability. An increase of permeability means an increase of the flux inside the source rock. Moreover, a strong variation of compaction inside the source rock can cause fractures which, in turn, induce the increase of permeability.

This thesis was carried out in collaboration with Eni S.p.A. An internship period was dedicated to the study of the effects of different retention models on the simulations of generation and primary migration of hydrocarbons, with deep insight into those retention process referred to as *adsorption* in mineral nanopores. Although in the model proposed in the present thesis these kind of processes are neglected for the sake of simplicity, this investigation will be very valuable when the model will be improved to include retention processes and more complex chemical kinetics for the generation of hydrocarbons. Hence, an appendix is dedicated to the illustration and comparison of the most common adsorption models in literature.

Compared to other problems related to oil exploration, the literature about the numerical simulation of the combined dynamic of oil generation and oil flow is quite limited. One of the main issues of the models of primary migration is that the porosity of the medium varies not only in space but also in time due to the conversion of the organic matter into fluid products. The model for the evolution of porosity in source rocks was first advanced in [21] and [20] by Wangen, who also proposed the idea of studying the problem in an artificial fixed domain, which we will follow in this thesis.

The work is structured as follows. In section 2 we give a general introduction on the processes that give origin to petroleum and to its accumulation in the reservoirs, following [1].

In section 3 we derive a new porosity law which accounts for the mutual interaction between mechanical compaction and kerogen dissolution effects. In particular, from the equation of mass conservation for the solid matrix we obtain the relationship between the rate of conversion from solid to fluid and the variation of kerogen concentration. Starting from this relation, we derive the new porosity law. Then, we present the model in the physical domain for a simplified source rock, which only consists of rock with no hydrocarbon potential and pure kerogen. For the sake of simplicity, we make the assumption that kerogen only generates oil and we use the two-phase Darcy model. Because of the consumption of kerogen and of the compaction of the rock due to the vertical pressure, the sediment matrix is not fixed and the physical domain moves. An original issue is that of studying and numerically solving the equations in a fixed domain, obtained

from the physical one as its completely compacted configuration, having removed all the degradable part of the rock. The advantage of writing the equations and solving the problem on a domain that, differently than the physical one, is fixed is that we do not need to deform the mesh according to the movement of the domain. The mesh can be built once and for all at the beginning of the simulation, as well as the basis functions of the finite element methods.

In section 4 we propose a strategy for the numerical solution of the system of equations. We first analyze each of the equations separately. Then, we propose an iterative strategy to solve the whole problem. Although a fully coupled approach is possible in principle, the two-phase Darcy model is decoupled via a common splitting technique in reservoir simulations, called IMPES. The equation for the oil phase saturation, which expresses a mass balance for the hydrocarbons in the source rock, is an advection-diffusion-reaction equation with degenerate diffusion. Its approximation is based on an ADR operator splitting, which allows to solve the advection part as a nonlinear conservation law via Godunov method, and the diffusion part exploiting the expanded finite element method, advanced by Chen in [3].

In section 5 we report some numerical results obtained by implementing the proposed strategy. The code was implemented with the support of *GetFEM++*, a `C++` finite element library.

Finally, three appendices are present. Appendix A illustrates the Piola transformation of vectorial fields, a tool that we use when reformulating the equations in the fixed domain. Appendix B is a brief summary of the main properties of the Raviart-Thomas finite elements used to approximate the Darcy problem as well as the parabolic part of the saturation equation. In appendix C we illustrate the phenomenon of adsorption and compare some common adsorption models.

2 Origin, migration and accumulation of petroleum

The origin of petroleum is never in the reservoir accumulation where it is discovered by exploration. Instead, prior to accumulation in the reservoir, petroleum has experienced a long series of processes, which happen if the following geological conditions are met:

- Occurrence of *source rocks* which generate petroleum (both oil and gas) under proper temperature conditions.

- Sediment compaction leading to expulsion of petroleum from the source rocks (*primary migration*).

- Occurrence of reservoir rocks of sufficient porosity and permeability allowing flow of petroleum through the pore system (*secondary migration*).

- Structural configurations of sedimentary strata where the reservoir rocks form traps, which should be sealed above by impermeable sediment layers.

- Favorable conditions for the preservation of petroleum accumulation during extended periods of time.

2.1 Deposition of source rock sediments

A petroleum source is characterized by three essential conditions. It must have a sufficient content of finely dispersed organic matter of biological origin; this organic matter must be rich in hydrogen; the source rock must be buried at certain depths and subject to proper temperatures to initiate the process of petroleum generation by the thermal degradation of kerogen. The organic carbon concentration is proved to be an approximate measure of the organic matter content of a rock. The minimum concentration of organic carbon for a productive source rock depends on the internal storage capacity of the rocks in terms of their porosity. If too little organic matter is present, the small quantities of petroleum generated will not exceed the storage capacity of the rock and no petroleum expulsion will take place.

The formation of sediments rich in organic matter is restricted to certain conditions of the depositional environment. These sediments are deposited in aqueous environments which receive a certain contribution of organic matter, such as residues of dead organisms and algae, along with the sediment particles. Instead, in a terrestrial environment, organic matter is readily destroyed by chemical and microbial oxidation shortly after deposition. All the aqueous depositional environments can also receive a supply of organic matter derived from higher land plants transported by rivers or glaciers, or simply wind-blown. In contrast to algal or bacterial biomass which is rich

in hydrogen, land plant-derived organic matter tends, due to high fractions of cellulose and lignin-derived materials, to be rich in oxygen. The organic matter of most source rocks is a mixture of residues derived from marine organisms as well as from terrestrial vegetation. It is the relative abundance of each of these organic materials which determines whether the resulting source rock will generate predominantly oil or gas upon burial.

The solid organic matter in source rocks is called *kerogen*. A useful geochemical approach for determining the complex composition of kerogen consists, as discussed in [19], in considering the relationship between the atomic hydrogen/carbon ratio H/C and the atomic oxygen/carbon ratio O/C (see figure 1).
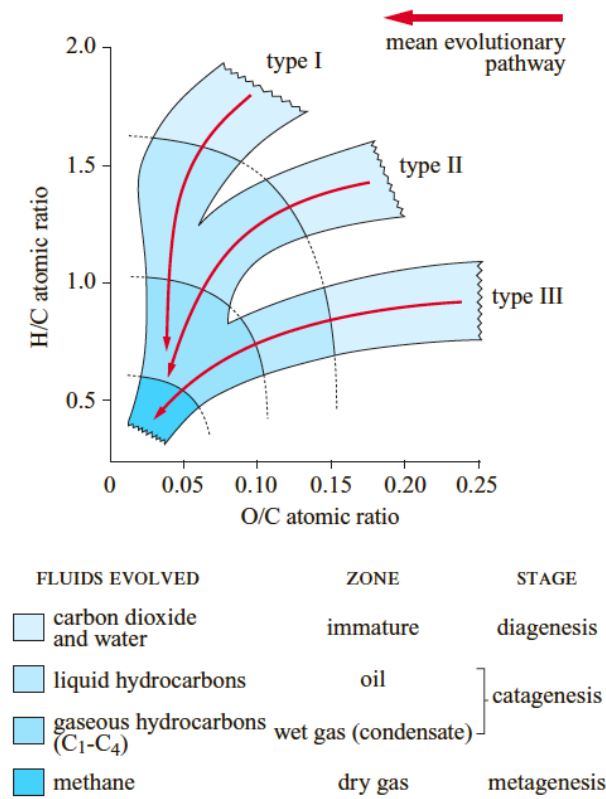
Figure 1: *Classification of kerogens into three broad categories in terms of their atomic H/C and O/C ratios. From the freshly deposited sediments (diagenesis stage), with increasing burial, kerogen transformation proceeds during the catagenesis and metagenesis stages. Figure from [1].*

Most prolific source rocks for oil have type II-kerogens. Type I-kerogens are rare, while source rocks of type III-kerogen generate little oil but more gas.

2.2 Oil and gas generation

Oil and gas are generated by the thermal degradation of kerogen. With increasing burial, the temperature in these rocks rises and, above a certain threshold temperature, the chemically labile portion of the kerogen begins to transform into petroleum compounds. The main reaction mechanism is the breaking of carbon-carbon bonds (*cracking*), which requires that the input of thermal energy exceeds certain minimum levels (activation energy). The generation of oil and gas in source rocks is a natural consequence of the increase of subsurface temperature during geologic time. The process of kerogen transformation with increasing temperature is called *maturation*, which is subdivided into the catagenesis and metagenesis stages. The organic matter is called *immature* prior to the onset of hydrocarbon generation, *mature* if hydrocarbon generation is in progress, *overmature* when these reactions have been terminated. The temperature interval where oil generation is in progress is referred to as the *oil window* and it extends over the temperature interval of about $80 - 150°$C. In the case of good quality source rocks, up to 50% of the kerogen is labile and converted into petroleum hydrocarbons while the source rock is in the oil window.

For petroleum exploration, it is essential to determine the precise stage at which hydrocarbon generation reactions have progressed in a particular source rock. This is done by measuring some maturation parameters. The most commonly used maturation parameter is *vitrinite reflectance*. With increasing maturation, the ability of vitrinite particles to reflect a beam of white light increases gradually. The oil window for source rocks with type II-kerogens extends over a maturity interval of about $0.5 - 1.3\%$ vitrinite reflectance. Above the maturity interval of $1.3 - 2.0\%$ vitrinite reflectance, lower molecular weight hydrocarbons in the form of condensates and wet gases are generated. At maturity levels in excess of 2.0% vitrinite reflectance, only dry gas is generated.

The ratio of the generated gas versus generated oil (GOR) depends on the type of its kerogen and its heating history during burial. Generally the gas to oil ratio increases with the increasing maturity of a source rock. In fact, methane is, thermodynamically, the most stable hydrocarbon species and the oil accumulations that get buried deeper and deeper and exposed to higher temperatures are ultimately converted into accumulations of dry gas by cracking processes.

2.3 Migration

The generation of petroleum by thermal degradation of kerogen is based on chemical processes controlled mainly by temperature. Instead, migration of petroleum from its place of origin in the source rock to its place of accumulation in the reservoir trap is controlled by the physical and physicochemical

conditions of the sedimentary strata the oil is moving through. Pressure exercises a major influence on this process. In the subsurface, we can identify two types of pressure. The *hydrostatic* pressure is the weight of the fluid column corresponding to the interconnected network of water-filled pores from a given depth up to the sediment surface, or sea surface for submerged basins. The *lithostatic* pressure is the sum of the weight of the rock column, transmitted from the surface to a given depth by grain-to-grain contacts, plus the weight of the pore fluid column. In a sedimentary basin, any deviation from the hydrostatic pressure is called an abnormal pressure. This can be *overpressure*, which is caused by the inability of pore fluids to escape from porous rocks in proportion with the overburden load, or *underpressure*.

Another set of physical and physicochemical conditions which exercise major control over the ability of petroleum to move through rocks are *porosity* and *permeability*. Porosity is the volume of void spaces as percentage of a given total volume of rock. For the applications of our interest, all pores in the subsurface are filled with water, with the exception of those situations where the pore water has been displaced by petroleum. Permeability characterizes the ability of fluids (water, oil, and gas) to move through porous rocks. Various relationships between porosity and permeability exist, depending on rock type. Finally, the movement of petroleum through porous rocks is influenced by capillary forces. This is due to the interfacial tension between two immiscible phases (oil/water or gas/water). The capillary pressure of a rock increases with decreasing pore size.

Primary migration

Primary migration of petroleum follows pressure gradients from the center of mature source rock towards the reservoir. The complex dynamics of primary migration are described in detail in [15]. One of the main driving forces for primary migration is sediment compaction due to overburden load. Compaction is achieved by the reduction of pore spaces with expulsion of pore water. Since oil is transported as a separate phase, any migrating oil phase has to overcome capillary pressures in the narrow pores of the originally water-wet source rocks. The effective flow can only be achieved once an interconnected network of oil-saturated pores has been established. It has been estimated that a minimum oil saturation of 20% has to be reached in the pores prior to initiation of its active flow. An additional mechanism to provide pressure for the expulsion of petroleum is due to the volume expansion associated to the conversion of solid labile kerogen into liquid and gaseous hydrocarbons. The newly generated hydrocarbons, which have entered these narrow pore spaces, cause the original pore fluid pressure to increase. If this rising pore fluid pressure reaches about 80% of the lithostatic pressure, the strength of the rock is exceeded and it fractures. Microfracture networks open and the expulsion of oil is facilitated.

The primary migration of natural gas components occurs mostly when they are dissolved in oil. In fact, at pressures exceeding the critical point in the phase diagram, oil and gas are present as a single-phase.

Secondary migration

As soon as the petroleum has entered the reservoir rock, quite different physical conditions prevail. Porosities, permeabilities and pore sizes are significantly higher. The main driving force of secondary migration is buoyancy which is due to the density contrast between petroleum hydrocarbons and water. A second driving mechanism can be hydrodynamic forces. The resisting force of capillary pressures counteracts these driving forces. Capillary pressure is the pressure which oil or gas has to overcome in order to displace the water from the pores of the rock it is trying to penetrate. If a rock has very narrow pore throats, capillary displacement pressure get so high that they cannot be exceeded by the buoyancy of the oil or gas and entrapment occurs.

The migration of petroleum continues as long as it does not encounter structural configurations where the reservoir strata form traps. For a trap to hold petroleum in place, it must be sealed by an impermeable cap rock. Under favorable pressure conditions, gas desorption will occur and a free gas phase will separate from the oil. Since gas has the highest buoyancy, it will accumulate at the top of the structure, forming the *gas cap*.

3 The model

3.1 The Darcy equation

Sediments and sedimentary rocks are porous media, i.e. solids that exhibit void spaces. These pores are normally connected and a fluid may flow through the void space. The way in which the pores are connected and their size determine how permeable a porous medium is for fluid flow, and the volume of the pore space controls its capacity to store fluid. The pores are a consequence of the variety of sizes and shapes of the grains the rocks consist of, but, as we are going to discuss later on, the pore space is also the result of a complex interplay of mechanical and chemical processes.

The assumptions that are usually made to identify a rock matrix as a porous medium are the following

- the void space of the solid matrix is interconnected;

- the dimensions of the pore space are large compared to the mean free path of fluid molecules. Under this assumption we are allowed to model the fluid in the void space as a continuum;

- the dimensions of the pores are small enough to consider the fluid flow as controlled by adhesive forces at fluid-solid interfaces and cohesive forces at fluid-fluid interfaces.

Under these hypotheses, we consider a domain $\Omega \in \mathbb{R}^d$ and define the functions:

$$\chi(\mathbf{x}, t) := \begin{cases} 1 \text{ if} & \mathbf{x} \in \text{ void space} \\ 0 \text{ if} & \mathbf{x} \in \text{ solid matrix} \end{cases} \qquad \mathbf{x} \in \Omega$$

and

$$\phi(\mathbf{x}, t, r) := \frac{1}{|\mathcal{B}_r(\mathbf{x})|} \int_{\mathcal{B}_r(\mathbf{x})} \chi(\mathbf{y}, t) \mathrm{d}\mathbf{y} \qquad \mathbf{x} \in \Omega,$$

where $\mathcal{B}_r(\mathbf{x})$ denotes the d-dimensional ball of center $\mathbf{x}$ and radius r. If there exists r_0 such that $|\frac{\partial \phi}{\partial r}| << 1$ for r in a neighborhood of r_0, then we define *porosity* the field $\phi(\mathbf{x}, t) = \phi(\mathbf{x}, t, r_0)$.

Darcy's law is an expression for the flux $\mathbf{U}$ of fluid that is flowing through a porous medium in response to a pressure gradient and is an approximation of the momentum conservation law. It postulates the existence of a *permeability* tensor field $\mathbf{K} \in \mathbb{R}^{d \times d}$, which is symmetric and positive definite, such that

$$\mathbf{U} = -\frac{1}{\mu} \mathbf{K} \left(\nabla p - \rho \mathbf{g} \right),$$

where $\mathbf{g}$ is the gravity acceleration $\mathbf{g} = -g\mathbf{e}_z$. Notice that in the vertical direction we have to subtract the effect of gravity: in fact, a fluid pressure equal to the weight of the fluid column leads to a zero Darcy flux.

The two parameters in Darcy's law are the permeability tensor $\mathbf{K}$, the fluid *viscosity* μ, and the fluid *density* ρ. The permeability is a rock property characterizing the rocks ability to conduct fluid and is determined by two main aspects: the size of the pores and how well the pores are connected.

The permeability has been measured for a large range of sediments and rocks, and it is a property that spans several orders of magnitude, as shown in figure 2.
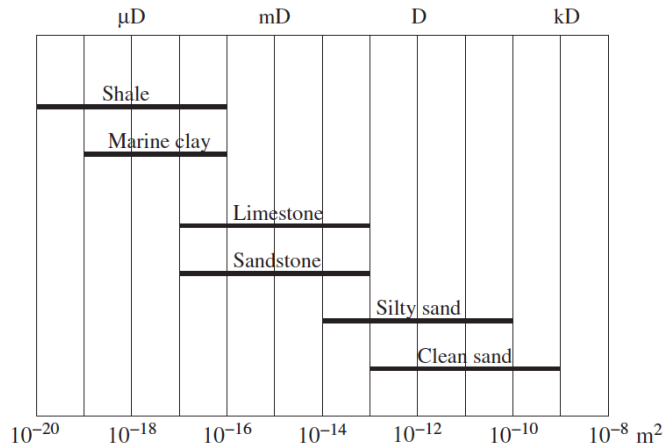
Figure 2: *The permeability for common sediments and sedimentary rocks. Notice that even the permeability of one rock type normally spans several orders of magnitude.*

Let us consider a fluid with two immiscible phases, e.g water w and oil o. For each phase $\alpha = w, o$ we define

$$\chi_\alpha(\mathbf{x}, t) := \begin{cases} 1 & \text{if} \quad \mathbf{x} \in \; \alpha \text{ phase} \\ 0 & \quad\quad \text{otherwise} \end{cases} \quad \mathbf{x} \in \Omega,$$

and

$$S_\alpha(\mathbf{x}, t, r) := \frac{\int_{\mathcal{B}_r(\mathbf{x})} \chi_\alpha(\mathbf{y}, t) \mathrm{d}\mathbf{y}}{\int_{\mathcal{B}_r(\mathbf{x})} \chi(\mathbf{y}, t) \mathrm{d}\mathbf{y}}$$

We then define *saturation* of phase α the function $S_\alpha(\mathbf{x}, t) := S_\alpha(\mathbf{x}, t, r_0)$, if there exists r_0 such that $|\frac{\partial S_\alpha}{\partial r}| << 1$ for r in a neighborhood of r_0. Experiments have shown that, when two immiscible fluids share the pore space, the Darcy's law can be applied separately for each phase, with the addition of a proper coupling condition. This condition is due to the interfacial tension that occurs at the interface between two immiscible phases. The corresponding effect in porous media is named *capillary pressure*, which indicates an additional fluid pressure. The model arisen, detailed in section 3.3, is the two-phase Darcy model, which also requires that the two phases completely fill the porous medium, that is $S_w + S_o = 0$.

3.2 Mechanical compaction under geochemical transformation

The objective of this section is to outline a mathematical model for compaction in source rocks that accounts for the degradation of kerogen. The model that we are going to deduce is rather general and accounts for all processes that involve conversion to liquid of part of the solid matrix.

Let us introduce some basic hypotheses, besides the classical ones for Darcy-type flows in porous media. The first is that the compaction process is governed by the same basic mechanisms that give rise (when only mechanical compaction is present) to the Athy's law of mechanical compaction. In particular, this means that the compaction process is relatively "slow".

The second hypothesis is that the kerogen can be considered as dispersed in the solid matrix. Indeed we assume that at any point $\mathbf{x}$ inside the domain and at any time t we can define a field $C = C(\mathbf{x}, t)$ that represents the ratio between the volume of kerogen and the initial rock volume, i.e. the solid volume when no degradation of kerogen has yet occurred.

We also make the usual assumption that the compaction acts only vertically. The extension to more general situations is possible but, because of its complexity, is beyond the scope of this thesis.

We first recall the basic derivation of Athy's law for mechanical compaction.

3.2.1 Athy's law for mechanical compaction

Athy's compaction law associates the porosity ϕ to the (vertical) effective stress $\sigma_e = \sigma_T - p$, where σ_T is the overload and p the pore pressure.

Athy's law reads

$$\phi(\boldsymbol{x}, t) = \phi_0 e^{-\beta \sigma_e(\boldsymbol{x}, t)}, \tag{1}$$

where ϕ_0 is the reference porosity (the porosity at $\sigma_e = 0$, that corresponds to uncompacted sediments) and β is a constant, typically fitted by experiments.

Notice that the condition $\sigma_e > 0$ implies that $0 \leq \phi \leq \phi_0$. Thus, if the reference porosity is in $[0, 1]$, then ϕ will be in $[0, 1]$ too.

In case the porous material exhibits hysteresis, a possibility is to assume that the compaction is linked to the maximum effective stress experienced by the material. This means replacing (1) with

$$\phi(\boldsymbol{x}, t) = \phi_0 e^{-\beta M(\sigma_e)(\boldsymbol{x}, t)}, \tag{2}$$

where

$$M(\sigma_e)(\boldsymbol{x}, t) = \sup_{\tau \in (0, t)} \sigma_e(\boldsymbol{y}(\tau), \tau) \tag{3}$$

and $\boldsymbol{y}(\tau)$ is the solid particle trajectory defined by

$$\begin{cases} \frac{d}{dt}\boldsymbol{y}(\tau) = \boldsymbol{u}(\boldsymbol{y}(\tau), \tau) & \tau \in (0, t) \\ \boldsymbol{y}(t) = \boldsymbol{x} \end{cases} \tag{4}$$

In the following derivation we will neglect hysteresis effects.

3.2.2 Standard derivation of Athy's law

Athy's compaction law associates the porosity ϕ to the effective vertical stress $\sigma_e = \sigma - p$, where σ is the overload and p is the pore pressure. Athy's law can be formally derived by assuming a *poroelastic* behavior described by

$$\frac{D\sigma_e}{Dt} = -\kappa(\xi)\nabla \cdot \boldsymbol{u}_s. \tag{5}$$

Here D/Dt indicates the material derivative, i.e. the derivative along the solid particle trajectory (4), and $\boldsymbol{u}_s$ is the solid velocity. We denote with ξ the solid volume fraction, that is related to the porosity by the equation $\xi = 1 - \phi$. Finally, κ is a viscosity parameter, which is, in general, function of the porosity ϕ. To derive Athy's law we consider the balance of mass for the solid fraction, assuming only mechanical compaction. If $V_s = V_s(t)$ is a solid material volume contained in our domain (i.e. a volume formed by the same solid particles), *for an incompressible material* we have

$$\frac{d}{dt}\int_{V_s(t)} \xi(\boldsymbol{x}, t)d\Omega = 0. \tag{6}$$

Standard application of Reynold's transport theorem gives, for $\boldsymbol{x} \in \Omega(t)$ and $t \in (0, T)$,

$$\frac{D\xi}{Dt}(\boldsymbol{x}, t) + \xi(\boldsymbol{x}, t)\nabla \cdot \boldsymbol{u}_s = 0, \tag{7}$$

by which, recalling that $\xi = 1 - \phi$,

$$-\frac{D\phi}{Dt} + (1 - \phi)\nabla \cdot \boldsymbol{u}_s = 0.$$

Combining the latter with (5) we obtain

$$\frac{D\sigma_e}{Dt} = -\frac{\kappa(\phi)}{1 - \phi}\frac{D\phi}{dt}. \tag{8}$$

Athy's law is easily recovered by choosing

$$\kappa(\phi) = \beta^{-1}\frac{1 - \phi}{\phi} \tag{9}$$

and integrating in time between 0 and t. Note that $\frac{1-\phi}{\phi}$ is the ratio between solid to pore volume.

3.2.3 Rock description and coordinates

Before extending the Athy's law to the case of kerogen degradation, we need to make some considerations about the domain of interest for our problem.

Because of the consumption of kerogen and of the compaction of the rock due to the vertical stress, the sediment matrix is not fixed and the domain $\Omega(t)$ in which we formulate the equations is time dependent. In order to avoid this complication and to write the equations on a fixed domain, following [21] we introduce the domains $\Omega^* = \Omega^*(t)$ and $\hat{\Omega}$, whose coordinates are indicated by (x, η) and (x, ξ) respectively. Notice that, since we assume that compaction leads only to a vertical movement of the solid matrix, all the domains have the same coordinate x. Ω^* is obtained from the actual domain $\Omega(t)$ as its completely compacted configuration, while $\hat{\Omega}$ is obtained from Ω^* removing all the degradable part of the rock (i.e. the kerogen). Thus, $\hat{\Omega}$ represents the volume occupied by non-degradable material *and is fixed* in time.

Let z be the vertical coordinate which has the layer bottom as the origin and ξ be the coordinate that measures the height of the non-kerogen part of the completely compacted source rock and has the layer bottom as the origin (see figure 3). Both the axes are oriented upwards.
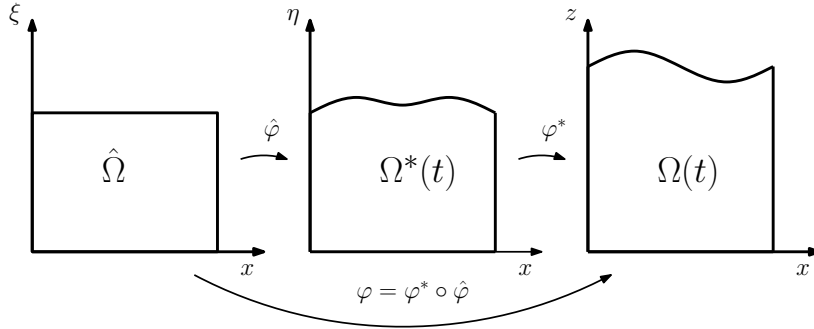
Figure 3: *The three coordinates systems. On the right, the physical domain $\Omega(t)$. Domain $\Omega^*(t)$ is obtained from $\Omega(t)$ as its completely compacted configuration, and domain $\hat{\Omega}$ is obtained from $\Omega^*(t)$ by removing all kerogen.*

As explained in [21], the map $\boldsymbol{\varphi} : \hat{\Omega} \to \Omega(t)$, $\boldsymbol{\varphi}(x, \xi) = (x, z(\xi, t))$ is

$$\boldsymbol{\varphi}(x, \xi) = \left(x, \quad -\int_{\xi}^{\xi^*} \frac{1 - C_0 + C(\xi')}{(1 - C_0)(1 - \phi(\xi'))} \mathrm{d}\xi' \right)$$

where ξ^* is the height of the basin along the ξ-axis and is computed from the porosity at the initial configuration.

In fact, in a small sediment volume measured to be $\mathrm{d}z$ high the amount of solid sediment is given by

$$\mathrm{d}\eta = (1 - \phi) \, \mathrm{d}z,$$

13

where ϕ is the porosity. $\mathrm{d}\eta$ measures the height of the sediment volume as completely compacted rock. If C represents the kerogen volume fraction of the initial solid part of the rock volume, the height of the volume measured as compacted rock without any kerogen is

$$\mathrm{d}\xi = (1 - C_0)\ \mathrm{d}\eta_0,$$

where C_0 is the initial kerogen fraction and $\mathrm{d}\eta_0$ is the initial amount of solid sediment $\mathrm{d}\eta_0 = (1 - \phi_0)\ \mathrm{d}z_0$. Thus, we have that

$$\mathrm{d}\eta = \mathrm{d}\xi + C\ \mathrm{d}\eta_0 = \left(1 + \frac{C}{1 - C_0}\right)\mathrm{d}\xi,$$

and

$$\mathrm{d}z = \frac{\mathrm{d}\eta}{1 - \phi} = \frac{1 - C_0 + C}{(1 - C_0)(1 - \phi)}\mathrm{d}\xi \qquad (10)$$

The relationship between z and ξ is then

$$z(\xi) = -\int_{\xi}^{\xi^*} \frac{1 - C_0 + C(\xi')}{(1 - C_0)(1 - \phi(\xi'))}\mathrm{d}\xi',$$

where ξ^* is the height of the basin along the ξ-axis.

Let us consider

$$\mathbf{J} := \nabla\boldsymbol{\varphi} = \begin{bmatrix} 1 & 0 \\ 0 & \partial z/\partial \xi \end{bmatrix}$$

Thus,

$$J := \det(\mathbf{J}) = \frac{\partial z}{\partial \xi}.$$

Let us observe that, due to the choice of the reference configuration $\hat{\Omega}$, the time derivative of the map from the reference to the actual configuration coincides with the velocity of the solid matrix: $\frac{\partial \boldsymbol{\varphi}}{\partial t} = \mathbf{u}_s$. This property will be very important for our purpose of obtaining a more general porosity law.

Proposition 1. *The partial differential equation*

$$\frac{\partial g}{\partial t} + \nabla \cdot (g\mathbf{u}) = Q \qquad in\ \Omega(t) \times (0, T]$$

with $g = g(x, z, t)$ can be formulated in the fixed reference system $\hat{\Omega} \times (0, T]$ as

$$\frac{\partial(\hat{g}\hat{J})}{\partial t} + \hat{\nabla} \cdot (\hat{g}(\hat{\mathbf{u}} - \hat{\mathbf{u}}_s)) = \hat{Q}\ \hat{J} \qquad in\ \hat{\Omega} \times (0, T] \qquad (11)$$

where we have set, for a generic function f, $\hat{f} = f \circ \boldsymbol{\varphi}$, for a generic velocity vector $\hat{\mathbf{v}} = \hat{J}\ \hat{\mathbf{J}}^{-1}\mathbf{v} \circ \boldsymbol{\varphi}$, and we have defined the operator

$$\hat{\nabla} = \begin{pmatrix} \partial/\partial x \\ \partial/\partial \xi \end{pmatrix} = \mathbf{J}\nabla = \mathbf{J}\begin{pmatrix} \partial/\partial x \\ \partial/\partial z \end{pmatrix}.$$

Proof. Since $\frac{\partial \boldsymbol{\varphi}}{\partial t} = \mathbf{u}_s$, one has

$$\begin{aligned}
\frac{\partial g}{\partial t} + \nabla \cdot (g\mathbf{u}) &= \frac{\partial g}{\partial t} + \nabla \cdot (g\mathbf{u}_s) \quad + \nabla \cdot (g(\mathbf{u} - \mathbf{u}_s)) \\
&= \frac{Dg}{Dt} + g\, \nabla \cdot \mathbf{u}_s \quad + \nabla \cdot (g(\mathbf{u} - \mathbf{u}_s))
\end{aligned}$$

Integrating the equation

$$\frac{Dg}{Dt} + g\, \nabla \cdot \mathbf{u}_s + \nabla \cdot (g(\mathbf{u} - \mathbf{u}_s)) = Q$$

on a volume $V(t) \in \Omega(t)$ that moves with the solid matrix, and applying the transport theorem, we obtain

$$\frac{\mathrm{d}}{\mathrm{d}t} \int_{V(t)} g \mathrm{d}V + \int_{V(t)} \nabla \cdot (g(\mathbf{u} - \mathbf{u}_s)) \mathrm{d}V = \int_{V(t)} Q \mathrm{d}V$$

Changing coordinates in the integral, we get

$$\frac{\mathrm{d}}{\mathrm{d}t} \int_{\hat{V}} \hat{g} \hat{J} \mathrm{d}\hat{V} + \int_{\hat{V}} \hat{\nabla} \cdot (\hat{g}(\hat{\mathbf{u}} - \hat{\mathbf{u}}_s)) \mathrm{d}\hat{V} = \int_{\hat{V}} \hat{Q} \hat{J} \mathrm{d}\hat{V} \tag{12}$$

where we have set, for a generic function f, $\hat{f} = f \circ \boldsymbol{\varphi}$, for a generic velocity vector $\hat{\mathbf{v}} = \hat{J}\, \hat{\mathbf{J}}^{-1} \mathbf{v} \circ \boldsymbol{\varphi}$, and

$$\hat{\nabla} = \begin{pmatrix} \partial/\partial x \\ \partial/\partial \xi \end{pmatrix} = \mathbf{J}\nabla = \mathbf{J} \begin{pmatrix} \partial/\partial x \\ \partial/\partial z \end{pmatrix}.$$

Since $\hat{V}$ is fixed, in (12) the $\mathrm{d}/\mathrm{d}t$ operator can be taken under the integration sign. Then, due to the arbitrariness of $\hat{V}$,

$$\frac{\partial(\hat{g}\hat{J})}{\partial t} + \hat{\nabla} \cdot (\hat{g}(\hat{\mathbf{u}} - \hat{\mathbf{u}}_s)) = \hat{Q}\, \hat{J} \qquad \text{in } \hat{\Omega} \times (0, T]. \tag{13}$$

$\square$

3.2.4 Extension to the case of kerogen degradation

Athy's compaction law is, in its classical formulation, expressed as (1) and its classic derivation has been illustrated in a previous paragraph. In presence of solid-fluid conversions, if q is the volumetric rate of conversion of solid matter into fluid, the balance of mass (6) for the solid fraction in a material volume $V_s(t)$ becomes

$$\frac{\mathrm{d}}{\mathrm{d}t} \int_{V_s(t)} (1 - \phi(\mathbf{y}(t), t)) \mathrm{d}\Omega = -\int_{V_s(t)} q \mathrm{d}\Omega.$$

Thus, by Reynold's theorem,

$$-\frac{D\phi}{Dt} + (1 - \phi)\nabla \cdot \mathbf{u}_s = -q \quad \text{in } \Omega(t) \times (0, T],$$

and, using the same *poroelastic* law that we used in the classical derivation (equation (5)), it follows that

$$\frac{D\sigma_e}{Dt} = -\frac{\mathcal{K}(\phi)}{1-\phi}\left(\frac{D\phi}{Dt} - q\right).$$

Using again (9), we obtain

$$\frac{D\sigma_e}{Dt} = -\frac{\beta^{-1}}{\phi}\left(\frac{D\phi}{Dt} - q\right). \tag{14}$$

In equation (14), the volumetric rate of conversion of solid into fluid q is function of the porosity and of the kerogen concentration C. Once we have found how to express $q = q(\phi, C)$ we can integrate the differential equation (analytically or numerically) to obtain $\phi = \phi(\sigma_e, C)$. We intend to derive this relation.

For the sake of simplicity, we consider a two-dimensional domain with coordinate system (x, z), yet the derivation can be readily extended to the $3D$ case. In particular we consider a two-dimensional section of a source rock within a sedimentary basin. The rock is assumed to consist of three basic parts: pure rock with no hydrocarbon potential, pure kerogen where all kerogen may be broken down to oil, and a void part initially filled with water. The pure rock and the kerogen make up the solid sediment matrix. We point out that, due to the consumption of kerogen and to the mechanical compaction, the solid matrix evolves in time. In the two-dimensional domain $\Omega(t)$ that follows the vertical movement of the solid matrix, the mass conservation for the latter is

$$\frac{\partial}{\partial t}\left((1-\phi)\rho_s\right) + \frac{\partial}{\partial z}\left((1-\phi)\rho_s u_{sz}\right) = Q_s \qquad \text{in } \Omega(t) \times (0, T]. \tag{15}$$

where Q_s is a sink term that represents the breakdown of kerogen into oil.

The solid matrix density ρ_s that appears in (15) is the mean over the densities of the two solid components weighted with respect to the fraction of the whole rock they make up, i.e $1 - C_0$ for pure rock and C for pure kerogen. Thus, ρ_s is related to the volume fraction of kerogen by the following equation:

$$\rho_s = \frac{(1 - C_0)\rho_r + C\rho_k}{1 - C_0 + C} \tag{16}$$

where ρ_r and ρ_k are the densities of the rock with no hydrocarbon potential and of kerogen, respectively, and C_0 is the initial volume fraction of kerogen. In this model $q = -\frac{Q_s}{\rho_k}$, hence we are interested in the relation $Q_s = Q_s(\phi, C)$.

From paragraph 3.2.3 it follows that equation (15) can be formulated in $\hat{\Omega} \times (0, T]$ as

$$\frac{\partial}{\partial t}\left((1-\hat{\phi})\hat{\rho}_s\hat{J}\right) = \hat{Q}_s\,\hat{J} \qquad \text{in } \hat{\Omega} \times (0, T]. \tag{17}$$

16

From equation (17) we can derive the relation $Q_s = Q_s(\phi, C)$ that we are looking for. In fact, since

$$\hat{J} = \frac{1 - C_0 + \hat{C}(x, \xi, t)}{(1 - C_0)(1 - \hat{\phi}(x, \xi, t))}, \tag{18}$$

equation (17) can be rewritten as

$$\frac{\partial}{\partial t}\left(\hat{\rho}_s \frac{1 - C_0 + \hat{C}(x, \xi, t)}{(1 - C_0)}\right) = \hat{Q}_s \, \hat{J} \quad \text{in } \hat{\Omega} \times (0, T].$$

Using equation (16), we obtain

$$\frac{\partial}{\partial t}\left(\rho_r + \frac{\hat{C}(x, \xi, t)}{1 - C_0}\rho_k\right) = \hat{Q}_s \, \hat{J} \quad \text{in } \hat{\Omega} \times (0, T].$$

Thus, since both ρ_r and ρ_k are constant, we obtain

$$\frac{1}{1 - C_0}\rho_k \frac{\partial \hat{C}}{\partial t} = \hat{Q}_s \, \hat{J} \quad \text{in } \hat{\Omega} \times (0, T].$$

Rearranging and substituting $\hat{J}$, we have

$$\hat{Q}_s = \rho_k \frac{(1 - \hat{\phi})}{1 - \hat{C}_0 + \hat{C}} \frac{\partial \hat{C}}{\partial t} \quad \text{in } \hat{\Omega} \times (0, T]. \tag{19}$$

which, brought back to the current domain provides the relation

$$Q_s = \rho_k \frac{(1 - \phi)}{1 - C_0 + C} \frac{DC}{Dt} \quad \text{in } \Omega(t) \times (0, T]. \tag{20}$$

Notice that $\frac{DC}{Dt} < 0$ due to the breakdown of kerogen, thus Q_s is a sink term for equation (15).

The volumetric rate of conversion of solid into fluid q in equation (14) is then given by

$$q = -\frac{Q_s}{\rho_k} = -\frac{1 - \phi}{1 - C_0 + C} \frac{DC}{Dt}.$$

The breakdown of kerogen is modeled as a first-order reaction of Arrhenius-type. The kerogen concentration C, defined as a volume fraction of the initial solid part of the rock sample, evolves as:

$$\frac{DC}{Dt} = -k \, C \quad \text{in } \Omega(t) \times (0, T], \tag{21}$$

where the reaction rate k is given by

$$k = Ae^{-E/RT}.$$

Here A is the Arrhenius factor, E is the activation energy, R is the gas constant, and T is the absolute temperature. Equation (21) is supplemented by the initial condition $C(\mathbf{x}, t) = C_0(\mathbf{x})$, where C_0 represents the initial kerogen volume fraction in the rock. Now, the differential equation (14) can be written as

$$\frac{D\sigma_e}{Dt} = -\frac{\beta^{-1}}{\phi}\left(\frac{D\phi}{Dt} - \frac{1-\phi}{1-C_0+C}k\,C\right), \tag{22}$$

which can be integrated explicitly, providing

$$\phi(\mathbf{x},t) = \left((1 + C(\mathbf{x},t) - C_0)\left(\phi_0 + \int_0^t \frac{kC(\mathbf{y}(\tau),\tau)e^{\beta\sigma_e(\mathbf{y}(\tau),\tau)}}{(1+C(\mathbf{y}(\tau),\tau)-C_0)^2}\mathrm{d}\tau\right)\right)e^{-\beta\sigma_e(\mathbf{x},t)}. \tag{23}$$

Again, here $\mathbf{y}(t)$ is the solid particle trajectory defined by (4). A crucial property for ϕ is that $\phi \in [0,1]$. In the following proposition we will prove that this important condition is guaranteed only under some restrictive hypotheses.

Proposition 2. *Let*

- $\phi_0(x,z) \in [0,1]\ \forall(x,z)\ \in \Omega(0)$,

- $C_0(x,z) \in [0,1]\ \forall(x,z)\ \in \Omega(0)$,

- $\frac{D\sigma_e}{Dt}(x,z,t) \geq 0$ *in* $\Omega(t) \times [0,T]$ *and* $\sigma_e(x,z,t) \geq 0$ *in* $\Omega(t) \times [0,T]$.

Let us set, $g(x,z,t) := 1 - (C_0(x,z) - C(x,z,t))$. *If*

$$\phi(x,z,t) = g(x,z,t)\left(\phi_0(x,z) + \int_0^t \frac{kC(\mathbf{y}(\tau),\tau)e^{\beta\sigma_e(\mathbf{y}(\tau),\tau)}}{(g(\mathbf{y}(\tau),\tau))^2}\mathrm{d}\tau\right)e^{-\beta\sigma_e(x,z,t)},$$

where $\mathbf{y}(t)$ *is the solid particle trajectory defined in (4), then* $\phi(x,z,t) \in [0,1]$ $\forall(x,z,t) \in \Omega(t) \times [0,T]$.

Proof. Let us prove that $\phi(x,z,t) \leq 1$ $\forall(x,z,t) \in \Omega(t) \times [0,T]$. Since $\sigma_e(x,z,t) \geq 0$,

$$\phi(x,z,t) \leq g(x,z,t)\left(\phi_0(x,z) + e^{-\beta\sigma_e(x,z,t)}\int_0^t \frac{kC(\mathbf{y}(\tau),\tau)e^{\beta\sigma_e(\mathbf{y}(\tau),\tau)}}{(g(\mathbf{y}(\tau),\tau))^2}\mathrm{d}\tau\right),$$

If $\frac{D\sigma_e}{Dt}(x,z,t) \geq 0$, then $e^{\beta\sigma_e(\mathbf{y}(\tau),\tau)} \leq e^{\beta\sigma_e(\mathbf{x},t)}$ $\forall\tau \in [0,t]$, where we recall that $\mathbf{y}(t) = \mathbf{x}$. Thus,

$$\phi(x,z,t) \leq g(x,z,t)\left(\phi_0(x,z) + \int_0^t \frac{kC(\mathbf{y}(\tau),\tau)}{(g(\mathbf{y}(\tau),\tau))^2}\mathrm{d}\tau\right) =: \tilde{\phi}(x,z,t).$$

18

$\tilde{\phi}(x, z, t)$ is the porosity that we have if $\sigma_e(x, z, \tau) = 0 \ \forall \tau \in [0, t]$, that is the porosity of the non compacted configuration. Computing the integral, recalling that $kC = -\frac{DC}{Dt}$, we obtain

$$\tilde{\phi}(x, z, t) = \phi_0(x, z) + (1 - \phi_0(x, z))(C_0(x, z) - C(x, z, t))$$

Since $1 - \phi_0 \geq 0$, $\tilde{\phi}$ is non-increasing in C. Then, the maximum value in time of the porosity corresponds to the minimum concentration, i.e. $C(x, z, t) = 0$. Once we have fixed one point $(x, z) \in \Omega(t)$, the maximum porosity in that point is

$$\max_{t \in [0, T]} \phi(x, z, t) = \phi_0(x, z) + C_0(x, z)(1 - \phi_0(x, z)) \leq 1 \quad \forall (x, z) \in \Omega(t),$$

because $C_0(x, z) \leq 1$.

Finally, to prove that $\phi(x, z, t) \geq 0 \ \forall (x, z, t) \in \Omega(t) \times [0, T]$, we notice that $C(x, z, t) \geq 0$ implies that $g \geq 1 - C_0(x, z) \geq 0$. Thus, all the factors in the definition of ϕ are non-negative. $\qquad \square$

3.2.5 Some considerations

In [21] a relation similar to (23) was found by Wangen with some heuristic arguments. However, the non-linear mutual interaction between mechanical compaction and dissolution process was neglected, leading to the following relation:

$$\phi = (\phi_0 + (1 - \phi_0)(C_0 - C)) \ e^{-\beta \ \sigma_e}. \tag{24}$$

However, this simpler relation may be recovered by setting $\sigma_e = 0$ in the expression under the integral in (23). Therefore, our relation may be seen as an *extension and generalization* of that of Wangen.

To better understand the relation between (23) and (24) let us introduce, for the sake of notation, the quantity

$$g = 1 - (C_0 - C). \tag{25}$$

It represents the ratio between the volume of solid at a given time and the initial one. Equation (24) can now be written as

$$\phi = (1 - g(1 - \phi_0))e^{-\beta \sigma_e} \tag{26}$$

while (23) may be rewritten as

$$\phi = g \left(\phi_0 - \int_0^t \frac{e^{\beta \sigma_e}}{g^2} \frac{dC}{d\tau} d\tau \right) e^{-\beta \sigma_e} \tag{27}$$

First of all, we state the following

Proposition 3. *If σ_e is taken identically zero inside the integral in Equation (27), then the former relation is equivalent to (26).*

Proof. It is sufficient to note that under the hypothesis the integral reduces to $\int_0^t g^{-2} \frac{dC}{d\tau} \mathrm{d}\tau = [-g^{-1}]_0^t = 1 - g(t)$. Replacing the integral in (27) with this expression leads to the desired result. $\square$

This proposition sheds a light on the differences between the two formulations. Expression (24) was indicated in [21] without a clear explanation. It can now be interpreted as an approximation of (27) (and thus (23)) where the non linear interaction between mechanical and "chemical" compaction is neglected, in particular the fact that degradation occurs on a layer that has already compacted (and continuing to compact) has been ignored.

Of course expression (23) depends on the choice we have made to describe the kerogen degradation process, and in particular the definition of C and (21). The most basic equation is indeed (14), whose solution however requires to have an expression for q.

A question that may be asked is whether one can assume that during the compaction process the porosity is still a non-increasing function of σ_e even when degradation of the solid matrix is present, and, in that case, how this constraint can be enforced in a physically and numerically sound way. For a purely mechanical compaction, this hypothesis is supported by the fact that the compaction is slow and once the grains have deformed to fill the voids after an increase of the effective stress, they do not recreate the void if unloaded.

Even if a more precise analysis would be necessary, one may conjecture that the monotonicity is still reasonable if the degradation is as "slow" as the mechanical compaction processes. The grains will tend to fill the "holes" opened up by the degradation. It is questionable, however, if this is still true when the degradation is relatively fast.

The fact that we have obtained (by a rigorous derivation) an explicit law for the porosity allows us to adapt existing codes that use relations of the type $\phi = \phi(\sigma_e)$ to account for the new porosity change associated to degradation.

3.3 The governing equations in the moving domain

As we have anticipated, we consider a two-dimensional section of a sedimentary basin containing a source rock layer. The source rock is assumed to consist of three basic parts: pure rock with no hydrocarbon potential, pure kerogen (all kerogen may be broken down to oil), and a void part initially filled with water. The pure rock and the kerogen make up the solid sediment matrix. We point out that, due to the consumption of kerogen and to the mechanical compaction, the solid matrix evolves in time. In the two-dimensional domain $\Omega(t)$ that follows the movement of the solid matrix,

the mass conservation of the fluid species, water and oil, can be expressed as:

$$\frac{\partial}{\partial t}\left(\phi\rho_w S_w\right) + \nabla\cdot\left(\phi\rho_w S_w \mathbf{u}_w\right) = Q_w \qquad \text{in } \Omega(t)\times(0,T], \qquad (28)$$

$$\frac{\partial}{\partial t}\left(\phi\rho_o S_o\right) + \nabla\cdot\left(\phi\rho_o S_o \mathbf{u}_o\right) = Q_o \qquad \text{in } \Omega(t)\times(0,T]. \qquad (29)$$

where $\phi = \phi(x,z,t)$ is the porosity of the rock, $\rho_w = \rho_w(x,z,t)$ and $\rho_o = \rho_o(x,z,t)$ are the densities of water and oil, which may depend on temperature and pressure. $S_w = S_w(x,z,t)$ and $S_o = S_o(x,z,t) = 1 - S_w(x,z,t)$ are the saturations of water and oil, respectively, and $\mathbf{u}_w = \mathbf{u}_w(x,z,t)$ and $\mathbf{u}_o = \mathbf{u}_o(x,z,t)$ their velocities. Finally, Q_o is a source term that accounts for the generation of oil through the breakdown of kerogen. To a first approximation, one can assume that the consumption of kerogen in rock only generates oil, i.e. $Q_w = 0$.

The velocities $\mathbf{u}_o$ and $\mathbf{u}_w$ are given, with respect to $\mathbf{u}_s$, by the Darcy law as

$$\phi S_w(\mathbf{u}_w - \mathbf{u}_s) = -\frac{k_{r,w}\mathbf{K}}{\mu_w}\left(\nabla p_w - \rho_w \mathbf{g}\right) \qquad \text{in } \Omega(t)\times(0,T], \quad (30)$$

$$\phi S_o(\mathbf{u}_o - \mathbf{u}_s) = -\frac{k_{r,o}\mathbf{K}}{\mu_o}\left(\nabla p_o - \rho_o \mathbf{g}\right) \qquad \text{in } \Omega(t)\times(0,T], \quad (31)$$

with $\mathbf{g} = -g\mathbf{e}_z$. Here $k_{r,w}$ and $k_{r,o}$ are the relative permeabilities of the two phases and are given functions of the saturations. The relative permeabilities can be modeled by several expressions found in the specialized literature. In our model, we will employ the Brooks-Corey relative permeability curves, namely

$$k_{r,w}(S_w) = S_w^3, \qquad (32)$$

$$k_{r,o}(S_o) = S_o^2\left(1 - (1 - S_o)^2\right). \qquad (33)$$

Note that if the relative permeability of one phase vanishes, then that phase cannot flow. In (30) and (31), μ_w and μ_o denote the viscosities of the two phases, which may depend on temperature. $\mathbf{K}$ is the permeability tensor and depends on the porosity ϕ, according to the following relation:

$$\mathbf{K}(\phi) = \mathcal{K}(\phi)\begin{bmatrix} k_{xx} & k_{xz} \\ k_{zx} & k_{zz} \end{bmatrix} \qquad (34)$$

where, following [4],

$$\mathcal{K}(\phi) = \begin{cases} k_0\phi^3 & \text{if} \quad \phi \geq 0.1 \\ \dfrac{100\,k_0\phi^5}{(1-\phi)^2} & \text{if} \quad \phi < 0.1 \end{cases}.$$

In the two-phase Darcy model the pressures of the fluids fulfill

$$p_o - p_w = p_c.$$

The capillary pressure p_c is a given function of either S_w or S_o. Following Brooks-Corey, we choose

$$p_c(S_w) = p_D \ S_w^{-1/m},$$

where p_D is the entry pressure, which depends on the porous medium characteristics, and m depends on the pore size distribution and is large for single-grained materials, small for highly nonuniform materials.

In order to close the formulation of the problem, we need some more information: how the breakdown of kerogen makes up the source term for equation (29) (i.e. equation $Q_o = Q_o(\phi, C)$), and how the porosity ϕ of the rock depends on the overload and on the kerogen volume fraction (i.e. $\phi = \phi(\sigma_e, C)$). Both the equations were derived in paragraph 3.2.4. In fact, $Q_o(\phi, C) = -Q_s(\phi, C)$ and from equation (20) follows:

$$Q_o(\phi, C) = -\rho_k \frac{(1 - \phi)}{1 - C_0 + C} \frac{DC}{Dt} \quad \text{in } \Omega(t) \times (0, T],$$

where we recall that (equation (21))

$$\frac{DC}{Dt} = -k \ C \quad \text{in } \Omega(t) \times (0, T],$$

which leads to

$$Q_o(\phi, C) = \rho_k \frac{(1 - \phi)}{1 - C_0 + C} \ k \ C \quad \text{in } \Omega(t) \times (0, T], \tag{35}$$

The porosity is given by equation (23), that we report in the following equation

$$\phi = \left((1 + C - C_0) \left(\phi_0 + \int_0^t \frac{kC(\mathbf{y}(\tau), \tau)e^{\beta\sigma_e(\mathbf{y}(\tau), \tau)}}{(1 + C(\mathbf{y}(\tau), \tau) - C_0)^2} d\tau \right) \right) e^{-\beta\sigma_e}.$$

In this equation, $\sigma_e = \sigma_e(x, z, t)$ represents the vertical effective stress, which is the bulk pressure σ_T minus the fluid pressure p_f

$$\sigma_e = \sigma_T - p_f.$$

The fluid pressure is defined as a mean over the oil pressure p_o and the water pressure p_w weighted with respect to the the saturations, i.e.

$$p_f = S_o p_o + S_w p_w,$$

and the bulk pressure at depth z can be computed as the pressure due to the weight of sediments and the pore fluids, i.e.

$$\sigma_T(x, z, t) = \int_z^{z_{top}} [(1 - \phi)\rho_s + \phi\rho_f] \ g \ dz' + \sigma_{top}(t),$$

where σ_{top} is the overburden and may be variable in time. Finally, ρ_f is given by

$$\rho_f = S_o\rho_o + S_w\rho_w.$$

3.4 The governing equations in the fixed domain

As we have anticipated, it is convenient to solve numerically the problem in the fixed domain $\hat{\Omega}$ introduced in section (3.2.3).

From equation (13), we derive the formulations of the mass conservation of the fluids in $\hat{\Omega}$. In this reference system the Darcy equations (30) and (31) become

$$\hat{\phi}\hat{S}_w(\hat{\mathbf{u}}_w - \hat{\mathbf{u}}_s) = -\hat{J}\frac{\hat{k}_{r,w}\hat{\mathbf{J}}^{-1}\mathbf{K}(\hat{\phi})}{\mu_w} \left(\hat{\mathbf{J}}^{-T}\hat{\nabla}\hat{p}_w - \rho_w\hat{\mathbf{g}}\right) \qquad \text{in } \hat{\Omega} \times (0, T]$$

$$\hat{\phi}\hat{S}_o(\hat{\mathbf{u}}_o - \hat{\mathbf{u}}_s) = -\hat{J}\frac{\hat{k}_{r,o}\hat{\mathbf{J}}^{-1}\mathbf{K}(\hat{\phi})}{\mu_o} \left(\hat{\mathbf{J}}^{-T}\hat{\nabla}\hat{p}_o - \rho_o\hat{\mathbf{g}}\right) \qquad \text{in } \hat{\Omega} \times (0, T]$$

because (see appendix A)

$$\begin{aligned}
\mathbf{u}_w - \mathbf{u}_s &= \hat{J}^{-1}\hat{\mathbf{J}}(\hat{\mathbf{u}}_w - \hat{\mathbf{u}}_s) \\
\mathbf{u}_o - \mathbf{u}_s &= \hat{J}^{-1}\hat{\mathbf{J}}(\hat{\mathbf{u}}_o - \hat{\mathbf{u}}_s)
\end{aligned} \tag{36}$$

and

$$\nabla p_w = \hat{\mathbf{J}}^{-T}\hat{\nabla}\hat{p}_w$$

$$\nabla p_o = \hat{\mathbf{J}}^{-T}\hat{\nabla}\hat{p}_o.$$

In the equations above, $\hat{\mathbf{g}} = -g\mathbf{e}_\xi$. Thus, the system we want to solve consists of the following equations in $\hat{\Omega} \times (0, T]$, where we have set $\hat{\mathbf{U}}_w = \hat{\phi}\hat{S}_w(\hat{\mathbf{u}}_w - \hat{\mathbf{u}}_s)$ and $\hat{\mathbf{U}}_o = \hat{\phi}\hat{S}_o(\hat{\mathbf{u}}_o - \hat{\mathbf{u}}_s)$

$$\frac{\partial(\rho_w\hat{\phi}\hat{S}_w\hat{J})}{\partial t} + \hat{\nabla} \cdot (\rho_w\hat{\mathbf{U}}_w) = 0 \tag{37}$$

$$\frac{\partial(\rho_o\hat{\phi}\hat{S}_o\hat{J})}{\partial t} + \hat{\nabla} \cdot (\rho_o\hat{\mathbf{U}}_o) = \hat{Q}_o\hat{J} \tag{38}$$

$$\hat{\mathbf{U}}_w = -\hat{J}\frac{\hat{k}_{r,w}\tilde{\mathbf{K}}}{\mu_w} \left(\hat{\nabla}\hat{p}_w - \rho_w\hat{\mathbf{J}}^T\hat{\mathbf{g}}\right)$$

$$\hat{\mathbf{U}}_o = -\hat{J}\frac{\hat{k}_{r,o}\tilde{\mathbf{K}}}{\mu_o} \left(\hat{\nabla}\hat{p}_o - \rho_o\hat{\mathbf{J}}^T\hat{\mathbf{g}}\right)$$

where we have set $\tilde{\mathbf{K}} := \hat{\mathbf{J}}^{-1}\mathbf{K}(\hat{\phi})\hat{\mathbf{J}}^{-T}$.

Recalling equations (18) and (35), we can write the right hand side of (38) as

$$\hat{Q}_o\hat{J} = k\frac{\hat{C}}{1-\hat{C}_0}\rho_k,$$

and

$$\frac{\partial \hat{C}}{\partial t} = -k\ \hat{C}.$$

Again, we have

$$\hat{S}_w + \hat{S}_o = 1,$$

$$\hat{p}_o - \hat{p}_w = p_c(\hat{S}_w),$$

where, for a generic function f, $\hat{f} := f \circ \boldsymbol{\varphi}$.

Finally, in the reference system, the equation for the bulk pressure becomes

$$\hat{\sigma}_T(x,\xi,t) = \int_{\xi}^{\xi_{top}} [(1-\hat{\phi})\hat{\rho}_s + \hat{\phi}\hat{\rho}_f]\hat{J}\ g\ \mathrm{d}\xi' + \sigma_{top}(t).$$

with

$$\hat{\rho}_s = \frac{(1-\hat{C}_0)\rho_r + \hat{C}\rho_k}{1-\hat{C}_0+\hat{C}}, \tag{39}$$

$$\hat{\rho}_f = \hat{S}_o\rho_o + \hat{S}_w\rho_w. \tag{40}$$

Initial and boundary conditions will be specified in next section.

4 The numerical solution

The aim of this section is to derive a numerical formulation for the equations in the fixed domain illustrated in section 3.4 and to advance a proper splitting strategy. From now on, we will omit the hats for the sake of convenience, yet referring to the equations in the fixed domain $\hat{\Omega}$. Let us introduce a triangulation $\mathcal{T}_h$ of the domain $\hat{\Omega}$. We assume, for the sake of simplicity, such that $\hat{\Omega}_h := \bigcup_{K \in \mathcal{T}_h} K = \hat{\Omega}$.

4.1 The global pressure formulation

Let us denote with $\mathbf{U}_\alpha$, p_α, and S_α the flux relative to the sediment particles, the pressure and the saturation of each phase with $\alpha = w, o$, respectively. The equations of the two-phase Darcy flow in the fixed domain are

$$\frac{\partial}{\partial t}(\rho_\alpha \phi S_\alpha J) + \nabla \cdot (\rho_\alpha \mathbf{U}_\alpha) = Q_\alpha J \qquad \hat{\Omega} \times (0, T], \tag{41}$$

$$\mathbf{U}_\alpha = -J \frac{k_{r,\alpha}}{\mu_\alpha} \tilde{\mathbf{K}} (\nabla p_\alpha - \rho_\alpha \mathbf{J}^T \mathbf{g}) \qquad \hat{\Omega} \times (0, T], \tag{42}$$

$$S_w + S_o = 1 \qquad \hat{\Omega} \times (0, T], \tag{43}$$

$$p_o - p_w = p_c(S_w) \qquad \hat{\Omega} \times (0, T]. \tag{44}$$

They can be written in and solved in an alternative, yet equivalent, formulation, the *Global Pressure Formulation*.

To obtain the Global Pressure Formulation, we introduce two artificial variables: the global pressure p and the total velocity $\mathbf{U} := \mathbf{U}_o + \mathbf{U}_w$. The equation for $\mathbf{U}$ can be obtained by adding together the two equations (41), which can be rewritten as

$$\nabla \cdot \mathbf{U}_\alpha = \frac{Q_\alpha J}{\rho_\alpha} - \frac{\partial}{\partial t}(\phi S_\alpha J) - \left(\phi S_\alpha J \frac{1}{\rho_\alpha} \frac{\partial \rho_\alpha}{\partial t} + \frac{\nabla \rho_\alpha}{\rho_\alpha} \cdot \mathbf{U}_\alpha \right).$$

If we can neglect the variations of the densities (in both space and time) and we assume that $\partial \rho_\alpha / \partial t$ and $\nabla \rho_\alpha$ are small with respect to ρ_α, we have

$$\nabla \cdot \mathbf{U} = \frac{Q_o J}{\rho_o} - \frac{\partial}{\partial t}(\phi J) \tag{45}$$

Now, adding the equations (42) together, we obtain

$$\mathbf{U} = -J \lambda_o \tilde{\mathbf{K}} (\nabla p_o - \rho_o \mathbf{J}^T \mathbf{g}) - J \lambda_w \tilde{\mathbf{K}} (\nabla p_w - \rho_o \mathbf{J}^T \mathbf{g})$$

where $\lambda_\alpha(S_\alpha) := \frac{k_{r,\alpha}(S_\alpha)}{\mu_\alpha}$ are the phase mobilities. We denote $\lambda(S_o) := \lambda_w(1 - S_o) + \lambda_o(S_o)$ as the total mobility. Exploiting equation (44) we have $\nabla p_w = \nabla p_o - \nabla p_c$, which, once inserted in the previous equation, provides

$$\mathbf{U} = -J \lambda \tilde{\mathbf{K}} \left(\nabla p_o - \frac{\lambda_w}{\lambda} \nabla p_c - \frac{\lambda_w \rho_w + \lambda_o \rho_o}{\lambda} \mathbf{J}^T \mathbf{g} \right). \tag{46}$$

The global pressure p is then defined as a scalar function such that

$$\nabla p = \nabla p_o - \frac{\lambda_w}{\lambda} \nabla p_c = \nabla p_o - \nabla \pi,$$

where

$$\pi(S_o) = \int_1^{S_o} \frac{\lambda_w(1 - \tilde{S})}{\lambda(\tilde{S})} p_c'(\tilde{S}) \mathrm{d}\tilde{S}.$$

We also introduce the vector modified gravity $\mathbf{G}$, defined as

$$\mathbf{G} := \frac{\lambda_w \rho_w + \lambda_o \rho_o}{\lambda} \mathbf{J}^T \mathbf{g}.$$

With this notation, equation (46) can be written as

$$\mathbf{U} = -J\lambda\tilde{\mathbf{K}} \left(\nabla p - \mathbf{G}\right). \tag{47}$$

The partial differential equation for one of the two saturation, e.g. for S_o, can be obtained by observing that equation (46) implies

$$\nabla p_o = -\frac{1}{J\lambda}\tilde{\mathbf{K}}^{-1}\mathbf{U} + \frac{\lambda_w}{\lambda}\nabla p_c + \mathbf{G}.$$

By inserting this expression for ∇p_o in equation (42) with $\alpha = o$, we obtain

$$\mathbf{U_o} = \frac{\lambda_o}{\lambda}\mathbf{U} - J\frac{\lambda_w \lambda_o}{\lambda}\tilde{\mathbf{K}} \left(\nabla p_c + (\rho_w - \rho_o)\mathbf{J}^T\mathbf{g}\right)$$

which can be coupled with equation (41) with $\alpha = o$ to provide an equation for the oil saturation.

The Global Pressure Formulation consists of the following equations:

| Global Pressure Formulation |

$$\begin{cases} \nabla \cdot \mathbf{U} = \dfrac{Q_o J}{\rho_o} - \dfrac{\partial}{\partial t}(\phi J) \\[2mm] \mathbf{U} = -J\lambda\tilde{\mathbf{K}} \left(\nabla p - \mathbf{G}\right) \end{cases} \tag{48}$$

$$\begin{cases} \dfrac{\partial}{\partial t}(\rho_o \phi S_o J) + \nabla \cdot (\rho_o \mathbf{U}_o) = Q_o J \\[2mm] \mathbf{U_o} = \dfrac{\lambda_o}{\lambda}\mathbf{U} - J\dfrac{\lambda_w \lambda_o}{\lambda}\tilde{\mathbf{K}} \left(\nabla p_c + (\rho_w - \rho_o)\mathbf{J}^T\mathbf{g}\right) \end{cases} \tag{49}$$

Notice that equations (48) are coupled with equations (49) through the function λ, which depend on the saturations. Once we have solved for $\mathbf{U}$, S_o and p, we can recover p_o and p_w as

$$p_o = p + \pi(S_o),$$
$$p_w = p + \pi(S_o) - p_c(1 - S_o).$$

When ϕ, Q_o, and J are given functions, a common way of solving the system of the Global Pressure Formulation is to operate a splitting, that decouples (48) from (49). In this way, known S_o^n, we can solve for $\mathbf{U}^{n+1}$ and p^{n+1}, as follows. Given the quantities at time step t^n, compute

$\boxed{\textbf{Pressure Equation}}$

$$\begin{cases} \nabla \cdot \mathbf{U}^{n+1} = \dfrac{Q_o J}{\rho_o} - \dfrac{\partial}{\partial t}(\phi J) \\ \quad \mathbf{U}^{n+1} = -J\lambda(S_o^n)\tilde{\mathbf{K}}\left(\nabla p^{n+1} - \mathbf{G}(S_o^n)\right) \end{cases}$$

then, using $\mathbf{U}^{n+1}$ we can solve for S_o^{n+1} the following nonlinear system:

$\boxed{\textbf{Saturation Equation}}$

$$\begin{cases} \dfrac{\partial}{\partial t}(\rho_o \phi S_o^{n+1} J) + \nabla \cdot (\rho_o \mathbf{U}_o^{n+1}) = Q_o J \\ \dfrac{\lambda_o(S_o^{n+1})}{\lambda(S_o^{n+1})}\mathbf{U}^{n+1} - J\dfrac{\lambda_w(S_o^{n+1})\lambda_o(S_o^{n+1})}{\lambda(S_o^{n+1})}\tilde{\mathbf{K}}\left(\nabla p_c + (\rho_w - \rho_o)\mathbf{J}^T\mathbf{g}\right) = \mathbf{U_o^{n+1}} \end{cases}.$$

This splitting strategy is known in literature as IMPES (i.e. IMplicit Pressure Explicit Saturation). In our case, since ϕ, Q_o, and J are unknown functions too, we will need a more complex splitting strategy, which still separates the pressure equation and the saturation one.

4.2 The pressure equation

In this paragraph we analyze the pressure equation and propose a solution strategy based on a finite element mixed method. Mixed methods have the advantage of approximating the velocity field as a variable of the problem, while in a classic formulation the velocity has to be computed by numerical differentiation of pressure. A direct computation of the velocity field is very convenient for the subsequent solution of the saturation equation. Moreover, since in a mixed formulation the continuity equation is not integrated by parts, we can also expect it to be satisfied with higher accuracy with respect to classic methods.

We consider the system

$$\begin{cases} \nabla \cdot \mathbf{U} = \dfrac{Q_o J}{\rho_o} - \dfrac{\partial}{\partial t}(\phi J) & \text{in } \hat{\Omega} \times (0, T] \\ \dfrac{1}{\lambda J}\tilde{\mathbf{K}}^{-1}\mathbf{U} = -(\nabla p - \mathbf{G}) & \text{in } \hat{\Omega} \times (0, T] \end{cases} \tag{50}$$

completed with the following set of boundary conditions:

$$\begin{cases} p = p_D & \text{on } \Gamma_D \\ \mathbf{U} \cdot \mathbf{n} = h & \text{on } \Gamma_N \end{cases}. \tag{51}$$

The Dirichlet boundary Γ_D and the Neumann boundary Γ_N are such that $\Gamma_D \cap \Gamma_N = \emptyset$ and $\Gamma_D \cup \Gamma_N = \partial\hat{\Omega}$. $\mathbf{n}$ is the normal to Γ_N pointing outwards.

Let us derive the weak formulation of this problem. Let us work formally first and test the equations against two sufficiently smooth test functions φ and $\boldsymbol{\tau}$. We will specify the functional setting later on.

We have

$$\int_{\hat{\Omega}} \nabla \cdot \mathbf{U} \, \varphi \, d\hat{\Omega} = \int_{\hat{\Omega}} \left(\frac{Q_o J}{\rho_o} - \frac{\partial}{\partial t}(\phi J) \right) \varphi \, d\hat{\Omega}$$

$$\int_{\hat{\Omega}} \frac{1}{\lambda J} \tilde{\mathbf{K}}^{-1} \mathbf{U} \cdot \boldsymbol{\tau} \, d\hat{\Omega} = - \int_{\hat{\Omega}} (\nabla p - \mathbf{G}) \cdot \boldsymbol{\tau} \, d\hat{\Omega}$$

Integrating by parts the right hand side of the second equation, we obtain

$$\int_{\hat{\Omega}} \frac{1}{\lambda J} \tilde{\mathbf{K}}^{-1} \mathbf{U} \cdot \boldsymbol{\tau} \, d\hat{\Omega} = \int_{\hat{\Omega}} p \, \nabla \cdot \boldsymbol{\tau} \, d\hat{\Omega} - \int_{\Gamma} p \, \boldsymbol{\tau} \cdot \mathbf{n} \, d\gamma + \int_{\hat{\Omega}} \mathbf{G} \cdot \boldsymbol{\tau} \, d\hat{\Omega}$$

If we assume that $\boldsymbol{\tau} \cdot \mathbf{n} = 0$ on Γ_N, we obtain the following equations:

$$\int_{\hat{\Omega}} \nabla \cdot \mathbf{U} \, \varphi \, d\hat{\Omega} = \int_{\hat{\Omega}} \left(\frac{Q_o J}{\rho_o} - \frac{\partial}{\partial t}(\phi J) \right) \varphi \, d\hat{\Omega}$$

$$\int_{\hat{\Omega}} \frac{1}{\lambda J} \tilde{\mathbf{K}}^{-1} \mathbf{U} \cdot \boldsymbol{\tau} \, d\hat{\Omega} - \int_{\hat{\Omega}} p \, \nabla \cdot \boldsymbol{\tau} \, d\hat{\Omega} = - \int_{\Gamma_D} p_D \, \boldsymbol{\tau} \cdot \mathbf{n} \, d\gamma + \int_{\hat{\Omega}} \mathbf{G} \cdot \boldsymbol{\tau} \, d\hat{\Omega}$$

If we approximate the term $\frac{\partial}{\partial t}(\phi J)$ as

$$\frac{\partial}{\partial t}(\phi J) \approx \frac{\Delta(\phi J)}{\Delta t},$$

where we indicate with $\Delta(\phi J)$ a proper variation of ϕJ over the time interval Δt (such as $\Delta(\phi J) = \phi^{n+1} J^{n+1} - \phi^n J^n$), the following functional setting guarantees that all the previous integrals make sense. Concerning the coefficients and the boundary conditions, we require that:

$$\boxed{\textbf{Assumptions on coefficients and boundary data}}$$

- $\phi, J, \rho_w, \rho_o, \mu_w, \mu_o \in L^\infty(\hat{\Omega} \times (0, T])$;

- $\tilde{\mathbf{K}} \in (L^\infty(\hat{\Omega} \times (0, T]))^{d \times d}$.
  If $\det(\tilde{\mathbf{K}}) \neq 0$, this condition implies $\tilde{\mathbf{K}}^{-1} \in (L^\infty(\hat{\Omega} \times (0, T]))^{d \times d}$;

- $Q_o \in L^2(\hat{\Omega} \times (0, T])$;

- $k_{ro}(S_o), k_{rw}(S_w) \in L^\infty(0, 1)$;

- $p_D, h \in L^2(0, T; H^{1/2}(\Gamma_D))$;

Let us introduce the space

$$H(\operatorname{div}; \hat{\Omega}) := \{\boldsymbol{\tau} \in (L^2(\hat{\Omega}))^d : \nabla \cdot \boldsymbol{\tau} \in L^2(\hat{\Omega})\}. \tag{52}$$

After the time discretization, a proper weak formulation for the pressure problem reads:

find $\mathbf{U}^{n+1} \in H(\operatorname{div}; \hat{\Omega})$ and $p^{n+1} \in L^2(\hat{\Omega})$ such that $\mathbf{U}^{n+1} \cdot \mathbf{n} = h$, and

$$\int_{\hat{\Omega}} \nabla \cdot \mathbf{U}^{n+1} \, \varphi \, d\hat{\Omega} = \int_{\hat{\Omega}} \left(\frac{Q_o J}{\rho_o} - \frac{\Delta(\phi J)}{\Delta t} \right) \, \varphi \, d\hat{\Omega}, \tag{53}$$

$$\int_{\hat{\Omega}} \frac{1}{\lambda J} \tilde{\mathbf{K}}^{-1} \mathbf{U}^{n+1} \cdot \boldsymbol{\tau} \, d\hat{\Omega} - \int_{\hat{\Omega}} p^{n+1} \, \nabla \cdot \boldsymbol{\tau} \, d\hat{\Omega} = - \int_{\Gamma_D} p_D \, \boldsymbol{\tau} \cdot \mathbf{n} \, d\gamma + \int_{\hat{\Omega}} \mathbf{G} \cdot \boldsymbol{\tau} \, d\hat{\Omega}, \tag{54}$$

$\forall \varphi \in L^2(\hat{\Omega})$ and $\forall \boldsymbol{\tau} \in H(\operatorname{div}; \hat{\Omega}) \cap \{\boldsymbol{\tau} : \boldsymbol{\tau} \cdot \mathbf{n} = 0\}$.

Notice that, while the Dirichlet boundary condition is included in the equations, the Neumann boundary condition needs to be embedded in the functional space setting.

Under proper regularity assumptions on the domain, the coefficients and the initial data, the well posedness of this problem can be proved (see [9]):

Proposition 4. *Let $\hat{\Omega}$ be an open bounded measurable subset of $\mathbb{R}^d$, with $d = 2$ or $d = 3$, with Lipschitz boundary $\partial\Omega$, and let $\Gamma_N \neq \emptyset$. Then problem (50)-(51) is well posed if, in addition to the previous assumptions on coefficients and boundary conditions, the following assumptions hold:*

- *There exist ϕ_1 and $\phi_2 \in \mathbb{R}^+$ such that $\phi_1 < \phi_2 < 1$ and $\phi_1 < \phi(\mathbf{x}, t) < \phi_2$ a.e. in $\hat{\Omega} \times (0, T)$.*

- *$\tilde{\mathbf{K}}$ is a symmetric positive definite tensor $\forall(\mathbf{x}, t) \in \hat{\Omega} \times (0, T]$ and there exists $K_0 \in \mathbb{R}^+$ such that $\|\tilde{\mathbf{K}}\|_{L^\infty(\hat{\Omega})} \geq K_0$.*

- *There exist $\rho_{o,0}$ and $\rho_{w,0} \in \mathbb{R}^+$ such that $\rho_\alpha \geq \rho_{\alpha,0}$ a.e. in $\hat{\Omega} \times (0, T)$, $\alpha = w, o$.*

- *There exist $\mu_{o,0}$ and $\mu_{w,0} \in \mathbb{R}^+$ such that $\mu_\alpha \geq \mu_{\alpha,0}$ a.e. in $\hat{\Omega} \times (0, T)$, $\alpha = w, o$.*

The finite dimensional spaces chosen for the numerical approximation are the lowest order Raviart Thomas elements $Z_h = \mathbf{RT}_0(\hat{\Omega}, \mathcal{T}_h) \subset H(\operatorname{div}, \hat{\Omega})$ for velocity, and the space of the piece-wise constant function $V_h = \mathbb{P}_0(\hat{\Omega}, \mathcal{T}_h) \subset L^2(\hat{\Omega})$ for pressure.

The Neumann boundary condition $\mathbf{U} \cdot \mathbf{n} = h$ on Γ_N, which is not included in the equations yet, will be imposed with Nitsche's penalization

technique (see [13]). Thus, we will add to the left hand side of equation (54) the term

$$\int_{\Gamma_N} \gamma_U (\mathbf{U} \cdot \mathbf{n})(\boldsymbol{\tau} \cdot \mathbf{n}) \, \mathrm{d}\gamma,$$

and to its right hand side the term

$$\int_{\Gamma_N} \gamma_U h(\boldsymbol{\tau} \cdot \mathbf{n}) \, \mathrm{d}\gamma.$$

The full discretization of the system is then given by

find $\mathbf{U}_h^{n+1} \in Z_h$ and $p_h^{n+1} \in V_h$ such that

$$\int_{\hat{\Omega}} \frac{1}{\lambda_h J_h} \tilde{\mathbf{K}}_h^{-1} \mathbf{U}_h^{n+1} \cdot \boldsymbol{\tau}_h \, \mathrm{d}\hat{\Omega} - \int_{\hat{\Omega}} p_h^{n+1} \, \nabla \cdot \boldsymbol{\tau}_h \, \mathrm{d}\hat{\Omega} + \int_{\Gamma_N} \gamma_U (\mathbf{U}_h^{n+1} \cdot \mathbf{n})(\boldsymbol{\tau}_h \cdot \mathbf{n}) \, \mathrm{d}\gamma$$

$$= -\int_{\Gamma_D} p_D \, \boldsymbol{\tau}_h \cdot \mathbf{n} \, \mathrm{d}\gamma + \int_{\hat{\Omega}} \mathbf{G}_h \cdot \boldsymbol{\tau}_h \, \mathrm{d}\hat{\Omega} + \int_{\Gamma_N} \gamma_U h(\boldsymbol{\tau}_h \cdot \mathbf{n}) \, \mathrm{d}\gamma,$$

$$\int_{\hat{\Omega}} \nabla \cdot \mathbf{U}_h^{n+1} \, \varphi_h \, \mathrm{d}\hat{\Omega} = \int_{\hat{\Omega}} \left(\frac{Q_{o\,h} J_h}{\rho_{o\,h}} - \frac{\Delta(\phi J)}{\Delta t} \right) \, \varphi_h \, \mathrm{d}\hat{\Omega},$$

$\forall \boldsymbol{\tau}_h \in Z_h$ and $\forall \varphi_h \in V_h$.

Proceeding with the usual technique, we write $\mathbf{U}_h^{n+1}$ and p_h^{n+1} using a proper base of the finite dimensional spaces Z_h and V_h

$$\mathbf{U}_h^{n+1} = \sum_j U_j^{n+1} \boldsymbol{\tau}_{hj} \qquad p_h^{n+1} = \sum_j p_j^{n+1} \varphi_{hj}$$

and require that the first equation holds for each $\boldsymbol{\tau}_{hi}$ of the base of Z_h and the second one holds for each φ_{hi} of the base of V_h, i.e.

$$\sum_j U_j^{n+1} \left(\int_{\hat{\Omega}} \frac{1}{\lambda_h J_h} \tilde{\mathbf{K}}_h^{-1} \boldsymbol{\tau}_{hj} \cdot \boldsymbol{\tau}_{hi} \, \mathrm{d}\hat{\Omega} \right) + \sum_j p_j^{n+1} \left(-\int_{\hat{\Omega}} \varphi_{hj} \, \nabla \cdot \boldsymbol{\tau}_{hi} \, \mathrm{d}\hat{\Omega} \right)$$

$$+ \sum_j U_j^{n+1} \left(\int_{\Gamma_N} \gamma_U (\boldsymbol{\tau}_{hj} \cdot \mathbf{n})(\boldsymbol{\tau}_{hi} \cdot \mathbf{n}) \, \mathrm{d}\gamma \right) = \int_{\Gamma_N} \gamma_U h(\boldsymbol{\tau}_{hi}\cdot\mathbf{n}) \, \mathrm{d}\gamma - \int_{\Gamma_D} p_D \, \boldsymbol{\tau}_{hi}\cdot\mathbf{n} \, \mathrm{d}\gamma + \int_{\hat{\Omega}} \mathbf{G}_h\cdot\boldsymbol{\tau}_{hi} \, \mathrm{d}\hat{\Omega}$$

$$\sum_j U_j^{n+1} \left(\int_{\hat{\Omega}} \nabla \cdot \boldsymbol{\tau}_{hj} \, \varphi_{hi} \, \mathrm{d}\hat{\Omega} \right) = \int_{\hat{\Omega}} \left(\frac{Q_{oh} J_h}{\rho_{oh}} - \frac{\Delta(\phi J)_h}{\Delta t} \right) \, \varphi_{hi} \, \mathrm{d}\hat{\Omega},$$

which can be written in the following algebraic form

$$\begin{bmatrix} A & B \\ -B^T & \mathbf{0} \end{bmatrix} \begin{bmatrix} \mathbf{U}^{n+1} \\ \mathbf{p}^{n+1} \end{bmatrix} = \begin{bmatrix} E \\ F \end{bmatrix},$$

with

$$A_{ij} = \int_{\hat{\Omega}} \frac{1}{\lambda_h J_h} \tilde{\mathbf{K}}_h^{-1} \boldsymbol{\tau}_{hj} \cdot \boldsymbol{\tau}_{hi} \, \mathrm{d}\hat{\Omega} + \int_{\Gamma_N} \gamma_U (\boldsymbol{\tau}_{hj} \cdot \mathbf{n})(\boldsymbol{\tau}_{hi} \cdot \mathbf{n}) \, \mathrm{d}\gamma,$$

$$B_{ij} = -\int_{\hat{\Omega}} \varphi_{hj} \, \nabla \cdot \boldsymbol{\tau}_{hi} \, \mathrm{d}\hat{\Omega},$$

$$E_i = \int_{\Gamma_N} \gamma_U h(\boldsymbol{\tau}_{hi} \cdot \mathbf{n}) \, \mathrm{d}\gamma - \int_{\Gamma_D} p_D \, \boldsymbol{\tau}_{hi} \cdot \mathbf{n} \, \mathrm{d}\gamma + \int_{\hat{\Omega}} \mathbf{G}_h \cdot \boldsymbol{\tau}_{hi} \, \mathrm{d}\hat{\Omega},$$

$$F_i = \int_{\hat{\Omega}} \left(\frac{Q_{oh} J_h}{\rho_{oh}} - \frac{\Delta(\phi J)_h}{\Delta t} \right) \varphi_{hi} \, \mathrm{d}\hat{\Omega}.$$

We introduce the linear operator $\mathcal{P}$ that associates the solutions $\mathbf{U}_h$ and p_h to the functions C_h, ϕ_h, S_{oh}, and $\Delta(\phi J)_h$

$$(\mathbf{U}_h^{n+1}, p_h^{n+1}) = \mathcal{P}(C_h, \phi_h, S_{oh}, \Delta(\phi J)_h).$$

It is interesting to point out that, if we assume that porosity is an unknown function, the Darcy problem (48) is actually a parabolic problem. In fact, the first equation of system (48) can be written as

$$\frac{\partial(\phi J)}{\partial p} \frac{\partial p}{\partial t} + \nabla \cdot \mathbf{U} = \frac{Q_o J}{\rho_o} - \frac{\partial(\phi J)}{\partial T} \frac{\partial T}{\partial t} - \frac{\partial(\phi J)}{\partial \sigma} \frac{\partial \sigma}{\partial t}. \tag{55}$$

where, if we use Athy's law for porosity,

$$\frac{\partial(\phi J)}{\partial t} = \beta \frac{1 - C_0 + C}{(1 - C_0)(1 - \phi)^2} (\phi_0 + (1 - \phi_0)(C_0 - C)) e^{-\beta \sigma_e}.$$

This term is a positive term, which would improve the stability of the numerical solution. Hence, a valid alternative to the numerical solution proposed consists of dealing with equation (55) instead of equation (48), which we discretize in time as follows:

$$\frac{\partial(\phi J)}{\partial p} \frac{p^{n+1} - p^n}{\Delta t} + \nabla \cdot \mathbf{U}^{n+1} = \frac{Q_o J}{\rho_o} - \frac{\partial(\phi J)}{\partial T} \frac{\partial T}{\partial t} - \frac{\partial(\phi J)}{\partial \sigma} \frac{\partial \sigma}{\partial t}.$$

4.3 The equation for the bulk pressure

We now consider equation

$$\sigma_T(x, \xi, t) = \int_{\xi}^{\xi_{top}} [(1 - \phi)\rho_s + \phi \rho_f] J g \, \mathrm{d}\xi' + \sigma_{top}(t)$$

for the bulk pressure σ_T. It is convenient to bring this equation back to its differential formulation. For this purpose, we derive this equation with respect to ξ and obtain the following differential problem:

$$\frac{\partial \sigma_T}{\partial \xi} = -((1 - \phi)\rho_s + \phi \rho_f) J g \quad \text{with} \quad \sigma_T(x, \xi_{top}, t) = \sigma_{top}(t).$$

We point out that the right hand side of the equation depends on the kerogen concentration C, on the saturation S_o, and on the porosity ϕ, since $\rho_s = \rho_s(C)$, $\rho_f = \rho_f(S_o)$, and $J = J(C, C_0, \phi)$. Thus, although there is no time derivative, the problem is indeed time dependent.

Multiplying the partial differential equation by a test function v, we have

$$\int_{\hat{\Omega}} \frac{\partial \sigma_T}{\partial \xi} v \, \mathrm{d}\hat{\Omega} = \int_{\hat{\Omega}} fv \, \mathrm{d}\hat{\Omega},$$

where in our case $f = -[(1 - \phi)\rho_s + \phi\rho_f]Jg$. For the assumptions made in paragraph 4.2, the right hand side of the stress differential equation is in $L^\infty(\hat{\Omega} \times (0, T])$.

The numerical solution of this problem required a stabilization. We propose the strongly consistent $SUPG$ stabilization, which consists of the addition of the term

$$\sum_{K \in \mathcal{T}_h} \delta h_K \int_K \left(\frac{\partial \sigma_T}{\partial \xi} - f \right) \frac{\partial v}{\partial \xi} \mathrm{d}K$$

to the integral formulation, where h_K is the dimension of the K-th element of the triangulation $\mathcal{T}_h$ and δ is a suitable parameter.

Hence, the stabilized weak formulation of the problem is:

find $\sigma_T^{n+1} \in H^1(\hat{\Omega})$ such that $\sigma_T^{n+1}(x, \xi_{top}) = \sigma_{top}(t^{n+1})$ and

$$\int_{\hat{\Omega}} \frac{\partial \sigma_T^{n+1}}{\partial \xi} v \, \mathrm{d}\hat{\Omega} + \sum_{K \in \mathcal{T}_h} \delta h_K \int_K \frac{\partial \sigma_T^{n+1}}{\partial \xi} \frac{\partial v}{\partial \xi} \mathrm{d}K = \int_{\hat{\Omega}} fv \, \mathrm{d}\hat{\Omega} + \sum_{K \in \mathcal{T}_h} \delta h_K \int_K f \frac{\partial v}{\partial \xi} \mathrm{d}K$$

$\forall v \in H^1(\hat{\Omega})$.

The discrete formulation is obtained by choosing the discrete space $S_h := \mathbb{P}_1(\hat{\Omega}, \mathcal{T}_h) \subset H^1(\hat{\Omega})$, and, following the usual procedure, one can write

$$\sigma_{Th}^{n+1} = \sum_j \sigma_j^{n+1} \varphi_{hj},$$

impose that the equation holds for each φ_{hi} of the base of S_h, and obtain the algebraic system:

$$\mathbf{A}\sigma^{n+1} = \mathbf{F}$$

where

$$A_{ij} = \int_{\hat{\Omega}} \frac{\partial \varphi_{hj}}{\partial \xi} \varphi_{hi} \, \mathrm{d}\hat{\Omega} + \sum_{K \in \mathcal{T}_h} \delta h_K \int_K \frac{\partial \varphi_{hj}}{\partial \xi} \frac{\partial \varphi_{hi}}{\partial \xi} \mathrm{d}K \qquad (56)$$

$$F_i = \int_{\hat{\Omega}} f\varphi_{hi} \, \mathrm{d}\hat{\Omega} + \sum_{K \in \mathcal{T}_h} \delta h_K \int_K f \frac{\partial \varphi_{hi}}{\partial \xi} \mathrm{d}K \qquad (57)$$

and σ^{n+1} is the vector of the coefficients of σ_{Th}^{n+1} with respect to the base chosen.

The Dirichlet boundary condition at ξ_{top} is imposed directly on the assembled matrix and right hand side vector, by eliminating from A and F the degrees of freedom corresponding to the Dirichlet nodes.

Let us define the linear operator Σ that associates to C_h, ϕ_h, and S_{oh} the numerical solution σ_{Th} to the stress problem whose coefficients are evaluated in C_h, ϕ_h, and S_{oh}:

$$\sigma_{Th} = \Sigma(C_h, \phi_h, S_{oh})$$

The discretization explained in this paragraph will also be used to solve numerically equation (15). In this case, we will take

$$f = Q_s - \frac{\Delta((1-\phi)\rho_s)}{\Delta t}$$

and the Dirichlet boundary conditions will be homogeneous and at $\xi = 0$.

4.4 The porosity equation

Let us consider the numerical computation of porosity. We recall that, in our model, the porosity is given by the following equation:

$$\phi(x, z, t) = \left((1 + C(x, z, t) - C_0) \left(\phi_0 + \int_0^t \frac{kC(\mathbf{y}(\tau), \tau)e^{\beta\sigma_e(\mathbf{y}(\tau),\tau)}}{(1 + C(\mathbf{y}(\tau), \tau) - C_0)^2} \mathrm{d}\tau \right) \right) e^{-\beta\sigma_e(x,z,t)}.$$

Let us indicate for the sake of notational convenience

$$s(t) := \frac{kC(\mathbf{y}(t), t)e^{\beta\sigma_e(\mathbf{y}(t),t)}}{(1 + C(\mathbf{y}(t), t) - C_0)^2}.$$

and let

$$\mathcal{I}^{n+1} := \int_0^{t^{n+1}} s(\tau)\mathrm{d}\tau.$$

The integral $\mathcal{I}^{n+1}$ can be approximated, applying the trapezoid method to each interval (t^k, t^{k+1}), i.e.

$$\mathcal{I}_h^{n+1} = \sum_{k=0}^{n} \frac{t^{k+1} - t^k}{2} (s(t^{k+1}) + s(t^k))$$

Thus, one can approximate the porosity at the instant t^{n+1} with

$$\phi_h^{n+1} = (1 + C_h - C_0) \left(\phi_0 + \mathcal{I}_h^{n+1} \right) e^{-\beta\sigma_{eh}}.$$

We define the linear operator Φ that associates to C_h and σ_{eh} the numerical computation of porosity ϕ_h, evaluated with C_h and σ_{eh}:

$$\phi_h = \Phi(C_h, \sigma_{eh}).$$

4.5 The saturation equation

The saturation equation is a nonlinear advection-diffusion-reaction equation, whose numerical solution is complicated by the degeneracy of the diffusion term at $S_o = 0$ and $S_o = 1$. As pointed out in [29], the solution of this problem has very low regularity. Indeed, it has been shown that

$$S_o \in L^\infty(0, T; L^1(\hat{\Omega})),$$

$$\frac{\partial S_o}{\partial t} \in L^2(0, T; H^{-1}(\hat{\Omega})).$$

Since the saturation satisfies $S_o(\mathbf{x}, t) \in [0, 1] \; \forall (\mathbf{x}, t) \in \hat{\Omega} \times (0, T]$, we have

$$S_o \in L^\infty(0, T; L^\infty(\hat{\Omega})).$$

The saturation equation will be approximated with an operator splitting approach. Since the equation is likely to be advection dominated, it is convenient to solve the advection part with a method tailored to hyperbolic problems, separately from the diffusion part. Let us indicate the advection, the diffusion and the reaction part of the equation explicitly. The saturation equation in $\hat{\Omega} \times (0, T]$ is:

$$\frac{\partial}{\partial t}(\rho_o \phi S_o J) = -\nabla \cdot (\rho_o \mathbf{U}_o) + Q_o J$$

$$\mathbf{U}_o = \frac{\lambda_o}{\lambda} \mathbf{U} - J \frac{\lambda_o \lambda_w}{\lambda} \tilde{\mathbf{K}} (\nabla p_c + (\rho_w - \rho_o) \mathbf{J}^T \mathbf{g})$$

with homogeneous Dirichlet boundary conditions on Γ_D, and homogeneous Neumann boundary conditions on Γ_N, and a proper initial condition $S_o(\mathbf{x}, 0) = S_0(\mathbf{x})$. Γ_D and Γ_N are such that $\Gamma_D \cap \Gamma_N = \emptyset$ and $\Gamma_D \cup \Gamma_N = \partial \hat{\Omega}$.

Substituting the second equation into the first one, we have

$$\frac{\partial}{\partial t}(\rho_o \phi S_o J) = -\nabla \cdot \left(\frac{\rho_o \lambda_o}{\lambda} \mathbf{U} - J \rho_o \frac{\lambda_o \lambda_w}{\lambda} \tilde{\mathbf{K}} (\rho_w - \rho_o) \mathbf{J}^T \mathbf{g} \right) + \nabla \cdot \left(\rho_o J \frac{\lambda_o \lambda_w}{\lambda} \tilde{\mathbf{K}} \nabla p_c \right) + Q_o J.$$

Let

$$\mathbf{F}(S_o) = \frac{\rho_o \lambda_o(S_o)}{\lambda(S_o)} \mathbf{U} - J \rho_o \frac{\lambda_o(S_o) \lambda_w(S_o)}{\lambda(S_o)} \tilde{\mathbf{K}} (\rho_w - \rho_o) \mathbf{J}^T \mathbf{g}$$

and

$$\mathbf{D}(S_o) = \rho_o J \frac{\lambda_o(S_o) \lambda_w(S_o)}{\lambda(S_o)} p_c'(S_o) \tilde{\mathbf{K}}.$$

Since $\nabla p_c(S_o) = p_c'(S_o) \nabla S_o$, the saturation equation is

$$\frac{\partial}{\partial t}(\rho_o \phi S_o J) = -\nabla \cdot \mathbf{F}(S_o) + \nabla \cdot (\mathbf{D}(S_o) \nabla S_o) + Q_o J.$$

We propose the following splitting strategy.

Advection:

$$\frac{\phi^* J^* S_o^{n+1/2} - \phi^n J^n S_o^n}{\Delta t} \rho_o = -\nabla \cdot \mathbf{F}(S_o^n),$$

Diffusion-Reaction:

$$\frac{\phi^* J^* S_o^{n+1} - \phi^* J^* S_o^{n+1/2}}{\Delta t} \rho_o = \nabla \cdot \left(\mathbf{D}(S_o^{n+1/2}) \nabla S_o^{n+1} \right) + Q_o J.$$
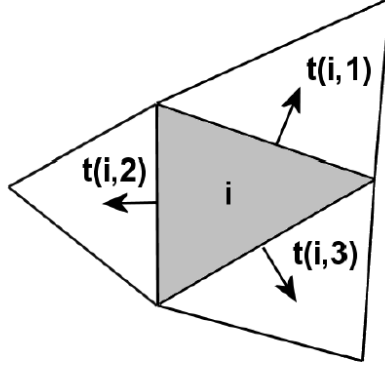

Figure 4: *The function $t(i, j)$ associated to the i-th element of the mesh, its j-th neighbor. In 2D, $j = 1, 2, 3$.*

We solve the advection step, by approximating the flux with a Godunov method. On the i-th element, we have

$$\nabla \cdot \mathbf{F}(S_o^n) \approx \frac{1}{A_i} \sum_{j=0}^{3} \mathcal{F}_{ij}(S_{o\ i}^n, S_{o\ t(i,j)}^n)$$

where $t(i, j)$ is the function that associates to element i its j-th neighbor (see figure 4), and $\mathcal{F}_{ij}$ is defined by

$$\mathcal{F}_{ij}(S_1, S_2) = \begin{cases} \min\limits_{S_1 \leq S_o \leq S_2} \int_j \mathbf{F}(z_i, S_o) \cdot \mathbf{n}_j \ \ \textit{if } S_1 < S_2 \\ \max\limits_{S_2 \leq S_o \leq S_1} \int_j \mathbf{F}(z_i, S_o) \cdot \mathbf{n}_j \ \ \textit{if } S_2 < S_1 \end{cases}$$

Using the Godunov method to solve the advection step, we have to verify that the mesh and the timestep are such that the CFL condition holds. More

precisely, we denote as ψ the conserved variable (in our case $\psi = \phi^* J^* S_o$) and with h_{K_i} the radius of element $K_i \in \mathcal{T}_h$. We define the CFL number on element K_i as

$$CFL_i = \max_{j \in t(i,j)} \max_{\mathbf{x} \in K_i} \frac{|\mathbf{F}'(\psi(\mathbf{x})) \cdot \mathbf{n}_j| \Delta t}{h_{K_i}}$$

and we have to make sure that $CFL := \max_i CFL_i < 1$. Notice that the derivative in the previous equation is a derivative with respect to the scalar variable ψ.

Under this condition, we compute $S_o^{n+1/2}$, which we approximate with a piece-wise constant, in each element of the mesh as

$$S_{oi}^{n+1/2} = \frac{\phi^n J^n}{\phi^* J^*} S_{oi}^n - \frac{\Delta t}{A_i \rho_o \phi^* J^*} \sum_{j=0}^{3} \mathcal{F}_{ij}(S_{o\ i}^n, S_{o\ t(i,j)}^n)$$

Concerning the solution of the diffusion-reaction step, we use a mixed finite element method. This will allow us to approximate S_o with a piece-wise constant function, and to avoid an interpolation of saturation between this step and the previous one.

Hence, we introduce an auxiliary variable $\boldsymbol{\sigma}^{n+1} = -\mathbf{D}(S_o^{n+1/2})\nabla S_o^{n+1}$, and the equation becomes

$$\frac{\phi^* J^* S_o^{n+1} - \phi^* J^* S_o^{n+1/2}}{\Delta t} \rho_o = -\nabla \cdot \boldsymbol{\sigma}^{n+1} + Q_o J.$$

The degeneracy of the the diffusion coefficient forbids to use mixed methods in their standard formulation. This criticality is avoided if we use the following *expanded* mixed finite element formulation proposed by Chen, in [3]. This formulation adds another auxiliary variable $\tilde{\boldsymbol{\sigma}}^{n+1} = \nabla S_o^{n+1}$ and approximates the solution of an equivalent system:

$$\begin{aligned}
\nabla \cdot \boldsymbol{\sigma}^{n+1} + \frac{1}{\Delta t}\rho_o \phi^* J^* S_o^{n+1} &= \frac{1}{\Delta t}\rho_o \phi^* J^* S_o^{n+1/2} + Q_o J \\
\tilde{\boldsymbol{\sigma}}^{n+1} - \nabla S_o^{n+1} &= 0 \\
\boldsymbol{\sigma}^{n+1} + \mathbf{D}(S_o^{n+1/2})\tilde{\boldsymbol{\sigma}}^{n+1} &= 0.
\end{aligned}$$

Multiplying these equations by the three test functions φ, $\boldsymbol{\tau}$ and $\boldsymbol{\nu}$ respectively, integrating over $\hat{\Omega}$, integrating by parts the second equation and applying the boundary condition, we have

$$\int_{\hat{\Omega}} \nabla \cdot \boldsymbol{\sigma}^{n+1} \varphi \, d\hat{\Omega} + \int_{\hat{\Omega}} \frac{1}{\Delta t}\rho_o \phi^* J^* S_o^{n+1} \varphi \, d\hat{\Omega} =$$

$$\int_{\hat{\Omega}} \left(\frac{1}{\Delta t}\rho_o \phi^* J^* S_o^{n+1/2} + Q_o J \right) \varphi \, d\hat{\Omega}$$

$$\int_{\hat{\Omega}} \tilde{\boldsymbol{\sigma}}^{n+1} \cdot \boldsymbol{\tau} \, d\hat{\Omega} + \int_{\hat{\Omega}} S_o^{n+1} \nabla \cdot \boldsymbol{\tau} \, d\hat{\Omega} + \int_{\Gamma_N} S_o^{n+1} \boldsymbol{\tau} \cdot \mathbf{n} \, d\gamma = 0$$

$$\int_{\hat{\Omega}} \boldsymbol{\sigma}^{n+1} \cdot \boldsymbol{\nu} \, d\hat{\Omega} + \int_{\hat{\Omega}} \mathbf{D}(S_o^{n+1/2})\tilde{\boldsymbol{\sigma}}^{n+1} \cdot \boldsymbol{\nu} \, d\hat{\Omega} = 0.$$

Under the assumptions on the regularity of the coefficients made in paragraph 4.2 and if the capillary pressure $p_c(S_o)$ is such that $p_c \in W^{1,\infty}(0,1)$, we can set the weak problem as follows:

find $S_o^{n+1} \in L^2(\hat{\Omega})$, $\boldsymbol{\sigma}^{n+1} \in H(\text{div}; \hat{\Omega})$, $\tilde{\boldsymbol{\sigma}}^{n+1} \in \left(L^2(\hat{\Omega})\right)^d$ such that the previous integral equations hold $\forall \varphi \in L^2(\hat{\Omega}), \forall \boldsymbol{\tau} \in H(\text{div}; \hat{\Omega})$ and $\forall \boldsymbol{\nu} \in \left(L^2(\hat{\Omega})\right)^d$.

Using the finite dimensional spaces $\mathbb{P}_0(\hat{\Omega}, \mathcal{T}_h) \subset L^2(\hat{\Omega})$, $\mathbf{RT}_0(\hat{\Omega}, \mathcal{T}_h) \subset H(\text{div}; \hat{\Omega})$, and $\mathbf{RT}_0(\hat{\Omega}, \mathcal{T}_h) \subset \left(L^2(\hat{\Omega})\right)^d$, choosing the base $\{\varphi_i\}_i$ of $\mathbb{P}_0(\hat{\Omega}, \mathcal{T}_h)$ and $\{\boldsymbol{\tau}_i\}_i$ of $\mathbf{RT}_0(\hat{\Omega}, \mathcal{T}_h)$, we can write the discrete problem in the algebraic form

$$
\begin{bmatrix} B^T & \mathbf{0} & M \\ \mathbf{0} & A & B+C \\ A & \tilde{A} & \mathbf{0} \end{bmatrix} \begin{bmatrix} \boldsymbol{\sigma} \\ \tilde{\boldsymbol{\sigma}} \\ \mathbf{S} \end{bmatrix} = \begin{bmatrix} \mathbf{E} \\ \mathbf{0} \\ \mathbf{0} \end{bmatrix},
$$

where

$$
A_{ij} = \int_{\hat{\Omega}} \boldsymbol{\tau}_i \cdot \boldsymbol{\tau}_j \qquad\qquad \tilde{A}_{ij} = \int_{\hat{\Omega}} \mathbf{D}(S_o^{n+1/2}) \boldsymbol{\tau}_j \cdot \boldsymbol{\tau}_i
$$

$$
B_{ij} = \int_{\hat{\Omega}} \nabla \cdot \boldsymbol{\tau}_i \, \varphi_j \qquad\qquad C_{ij} = \int_{\Gamma_N} \boldsymbol{\tau}_i \cdot \mathbf{n} \, \varphi_j
$$

$$
M_{ij} = \int_{\hat{\Omega}} \frac{1}{\Delta t} \rho_o \phi^* J^* \varphi_i \varphi_j \qquad E_i = \int_{\hat{\Omega}} \left(\frac{1}{\Delta t} \rho_o \phi^* J^* S_o^{n+1/2} + Q_o J \right) \varphi_i
$$

and $\mathbf{S}, \boldsymbol{\sigma}$, and $\tilde{\boldsymbol{\sigma}}$ are the coefficients of $S_{oh}^{n+1}, \boldsymbol{\sigma}_h^{n+1}$, and $\tilde{\boldsymbol{\sigma}}_h^{n+1}$ with respect to the chosen basis. Some rows of matrix $\tilde{A}$ can vanish when the diffusion term degenerates, yet the system is still invertible.

Let us define the linear operator $\mathcal{S}$ that associates to $C_h, \phi_h, \mathbf{U}_h, \phi_h^*$, and C_h^* the numerical solution S_{oh} to the saturation equation corresponding to $C_h, \phi_h, \mathbf{U}_h, \phi_h^*$, and C_h^*:

$$
S_{oh} = \mathcal{S}(C_h, \phi_h, \mathbf{U}_h, \phi_h^*, C_h^*).
$$

4.6   The concentration equation

The equation for the concentration

$$
\frac{\partial C}{\partial t} = -k \, C
$$

is solved numerically with an Implicit Euler scheme. We recall that k is time dependent, since it is a function of the temperature T, which here is a given

function that may depend on time. Thus, we have

$$\frac{C^{n+1} - C^n}{\Delta t} = -k(T^{n+1})\, C^{n+1}.$$

The full discretization of the problem is

$$C_h^{n+1} = \frac{1}{1 + \Delta t\ k(T^{n+1})}\, C_h^n,$$

where C_h^{n+1}, $C_h^n \in \mathbb{P}_0(\hat{\Omega}, \mathcal{T}_h)$.

We introduce the linear operator $\mathcal{C}$ that associates to C_h, the solution C_h^{n+1} of the discrete problem.

4.7 The splitting strategy

In this paragraph we describe the splitting strategy that we use in order to solve the whole problem. The initial conditions that we need are $C^0, \phi^0, \phi^{-1}, p^0, S_o^0, \mathbf{U}^0$, and σ_e^0. Notice that we need two initial conditions for porosity.

Known, $C^n, \phi^n, \phi^{n-1}, p^n, S_o^n, \mathbf{U}^n$, and σ_e^n, we solve the concentration equation, which is independent of the other variables. Thus,

$$C^{n+1} = \mathcal{C}(C^n).$$

We then solve the saturation equation and set

$$S_o^{n+1} = \mathcal{S}(C^{n+1}, \phi^n, \mathbf{U}^n, \phi^*, C^{n+1}),$$

where we choose $\phi^* = 2\phi^n - \phi^{n-1}$. Once obtained S_o^{n+1}, we can compute p_o^{n+1}, p_w^{n+1} and p_f^{n+1} from p^n, and ρ_f^{n+1} and ρ_s as

$$p_o^{n+1} = p^n - \pi_w(1 - S_o^{n+1})$$
$$p_w^{n+1} = p_o^{n+1} - p_c(1 - S_o^{n+1})$$
$$p_f^{n+1} = S_o^{n+1} p_o^{n+1} + (1 - S_o^{n+1}) p_w^{n+1}$$
$$\rho_f^{n+1} = S_o^{n+1} \rho_o^{n+1} + (1 - S_o^{n+1}) \rho_w^{n+1}$$
$$\rho_s^{n+1} = \frac{(1 - C^0)\rho_r + C^{n+1}\rho_k}{1 - C^0 + C^{n+1}}.$$

Then, we solve the stress equation by setting

$$\sigma_T^{n+1} = \Sigma(C^{n+1}, \phi^n, S_o^{n+1}).$$

We can compute the effective stress as $\sigma_e^{n+1} = \sigma_T^{n+1} - p_f^{n+1}$, and the porosity as

$$\phi^{n+1} = \Phi(C^{n+1}, \sigma_e^{n+1}).$$

Finally we compute the total velocity $\mathbf{U}^{n+1}$ and global pressure p^{n+1}:

$$\left(\mathbf{U}^{n+1}, p^{n+1}\right) = \mathcal{P}(C^{n+1}, \phi^{n+1}, S_o^{n+1}, \Delta(\phi J)),$$

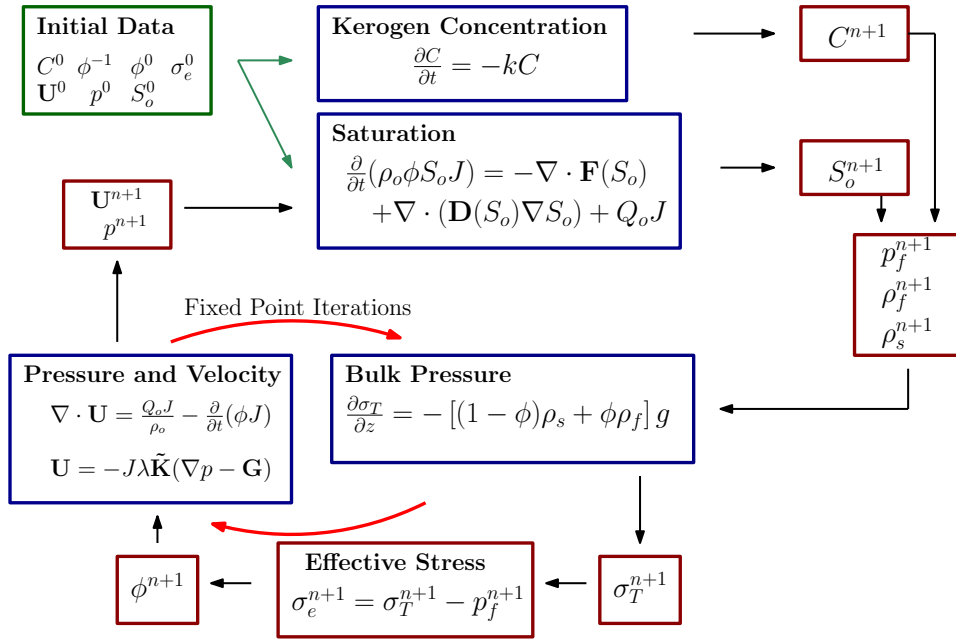where we choose $\Delta(\phi J) = \phi^{n+1} J(C^{n+1}, C^0, \phi^{n+1}) - \phi^n J(C^n, C^0, \phi^n)$.

Figure 5: *The splitting strategy that is used to solve the equations. Some fixed point iteration are necessary (see section 5.3).*

5 Results

The following tests were carried out in a 100 m squared domain $\hat{\Omega}$ initially at the depth of 2000 m, with a 30×30 regular triangular mesh built with the tools provided by $GetFEM++$. When necessary (i.e. in the test of Darcy and compaction and in the full test) the penalization and stabilization parameters were set equal to $\gamma_U = 5 \ 10^6$ and $\delta = 5 \ 10^4$, respectively. In the test cases where compaction is taken into account, a sedimentation velocity of 50 m per million years was set. The temperature, necessary to trigger the chemical reaction of kerogen degradation, is a given field that corresponds to a surface temperature of 20 °C and a geothermal gradient of 3.5 °C per 100 m. Finally, if we assume that the velocity of the oil phase outside the source rock is much higher than that inside the domain, therefore we can impose that only water is present at the boundaries (i.e. $S_o = 0$ on $\partial\hat{\Omega}$).

5.1 Test of Darcy problem and compaction

In this test we consider a rock only filled with water and with no kerogen $(C(\mathbf{x}, t) = C^0 = 0)$. Thus no oil can be generated $(S_o(\mathbf{x}, t) = S_o^0 = 0)$. The initial conditions for pressure consists of an hydrostatic pressure and the initial conditions for the effective stress and porosity are obtained with some fixed point iterations, starting from a uniform porosity equal to the porosity of the initial non compacted configuration $\phi_0 = 0.5$, computing the overload corresponding to that porosity, and computing the effective stress as the overload less the initial pore pressure. In this test we consider a progressive sedimentation of the layers above the domain during the 50 My of simulation. This fact causes a progressive burial of the domain, which causes the boundary conditions for both overload and pressure to change.

With the notation of section 4, at each time iteration, known ϕ^n, p^n, and σ_e^n, we solve the stress equation and set

$$\sigma_T^{n+1} = \Sigma(C^0, \phi^n, S_o^0).$$

We can compute the effective stress as $\sigma_e^{n+1} = \sigma_T^{n+1} - p_f^n$, and the porosity as

$$\phi^{n+1} = \Phi(C^0, \sigma_e^{n+1}).$$

Finally we compute the total velocity $\mathbf{U}^{n+1}$ and global pressure p^{n+1}:

$$\left(\mathbf{U}^{n+1}, p^{n+1}\right) = \mathcal{P}(C^0, \phi^{n+1}, S_o^0, \Delta(\phi J)),$$

where we choose $\Delta(\phi J) = \phi^{n+1} J(C^0, C^0, \phi^{n+1}) - \phi^n J(C^0, C^0, \phi^n)$.

Instability problems were observed with small time steps, i.e. $\Delta t \lesssim 10^{10}s$, so in this case, some fixed point iteration were necessary. These instabilities were observed to worsen with small permeability coefficients k_0. The stop condition used is based on the variations of the Jacobian $J(C, C^0, \phi)$,

which accounts for the movement of the physical domain. Thus, set $\mathbf{J}_k^{n+1}$ the vector of the DOFs of the finite element function $J(C^0, C^0, \phi_k^{n+1})$ we check for each fixed point iteration $k < K_{max}$ if

$$\frac{||\mathbf{J}_k^{n+1} - \mathbf{J}_{k-1}^{n+1}||_2}{||\mathbf{J}_k^{n+1}||_2} < tol,$$

We take a time step $\Delta t = 10^{13}$ and 150 time iterations.

In figure 6 we can clearly observe the progressive compaction of the physical domain. This compaction can also be observed in figure 7, as ϕ increases significantly from the beginning to the end of the simulation in the whole domain. We can also observe the behavior of porosity which, coherently with the behavior of the effective stress (see figure 8), is much lower at the top of the domain than at the bottom.
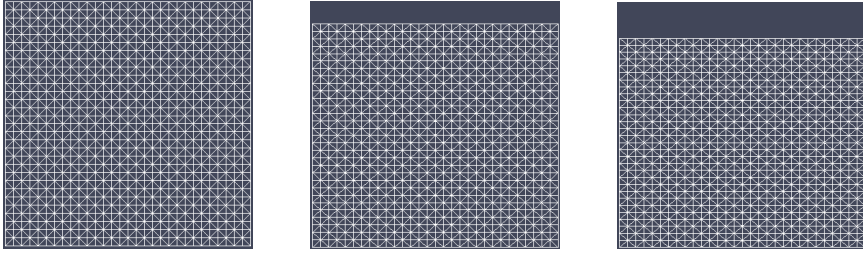
Figure 6: *The deformation of the physical domain. The three snapshots were taken at $t = 0$, $t = 27$ My and $t = 50My$.*

Figure 7: *The evolution of porosity ϕ. The two snapshots were taken at $t = 0$ and $t = 50$ My, i.e. at the beginning and at the end of the simulation.*
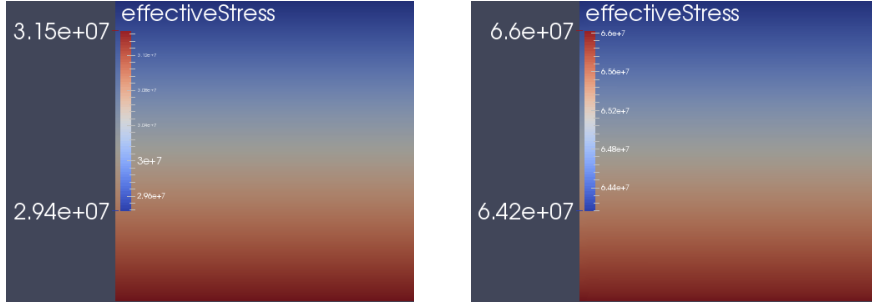
Figure 8: *The evolution of the effective stress σ_e. The two snapshots were taken at $t = 0$ and $t = 50$ My, i.e. at the beginning and at the end of the simulation.*

5.2 Test of the saturation problem

In this second test case, we consider a rock with no kerogen ($C(\mathbf{x}, t) = C^0 = 0$), initially filled with water, except for a bubble of oil. Porosity is assumed to be constant ($\phi(\mathbf{x}, t) = \phi^0 = 0.3$) and no sedimentation effects are considered. Finally, we set $\mathbf{U} = \mathbf{0}$, i.e. the velocity of the water phase has equal module but is opposite to that of the oil phase. Under these assumptions, we solve the saturation equation, in order to simulate the movement of the oil bubble.

Known S_o^n, we solve the saturation equation and set

$$S_o^{n+1} = \mathcal{S}(S_o^n, C^0, \phi^0, \mathbf{U}^0, \phi^0, C^0).$$

The time step used is $\Delta t = 10^{12} s$ and 1500 time iteration were performed. Thus 50 My are simulated.

In figure 9, we can notice that the oil bubble, being oil lighter than water, moves upward and goes out of the domain, leaving a contrail of intermediate saturation between oil ($S_o = 0$) and water ($S_o = 1$).
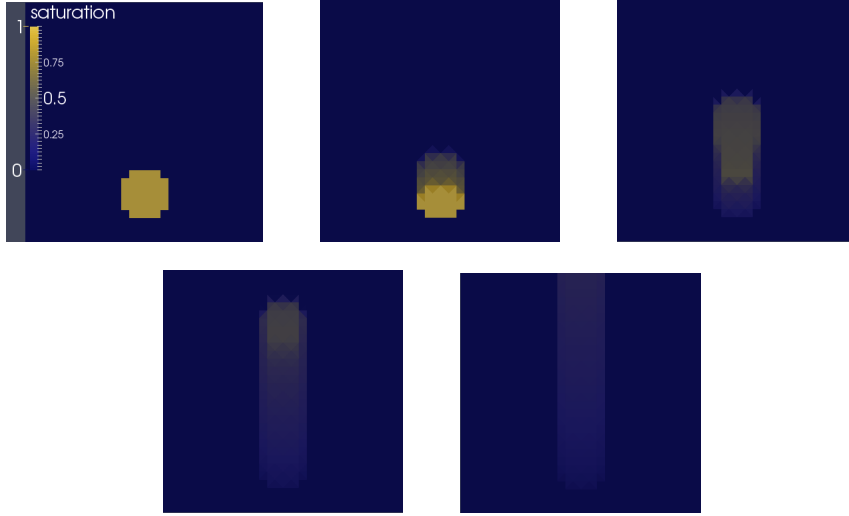
Figure 9: *The oil saturation at $t = 0$, $t = 4$ My, $t = 7$ My, $t = 14$ My, $t = 23$ My.*

5.3 Test of the full problem

This last test is a test of the full problem. Initially the rock is filled with water and the oil saturation is $S_o^0 = 0$. The initial condition for pressure is the hydrostatic pressure and the initial conditions for stress and porosity are computed with some fixed point iterations, starting from a uniform porosity equal to the porosity of the non-compacted configuration, $\phi_0 = 0.5$. We consider an initial brick of kerogen and an initial depth of 2000 m. Finally, $\mathbf{U}^0 = \mathbf{0}$ and $\phi^{-1} = \phi^0$. Notice that we need two initial conditions for porosity.

This test is conducted neglecting the effects of capillary pressure. Hence only the advection and reaction part of the saturation equation is considered.

We apply the splitting strategy described in section 4.7 (see figure 5).

As in the first test, in this case too some fixed point iterations of the stress-porosity-Darcy problem were necessary for the sake of stability. In fact, is this case the CFL condition forces a smaller time step than that in the first test case. 50 My were simulated with 1500 time iteration of $10^{12}s$ each.

The following figures represent the physical domain. The progressive compaction due to the increasing vertical stress is clear. We can also observe in the sketches correspondent to 50 My that the region of source rock with positive initial kerogen concentration compacts more than the neighboring regions. In figure 10, we zoom the upper region of the mesh at the last iteration.
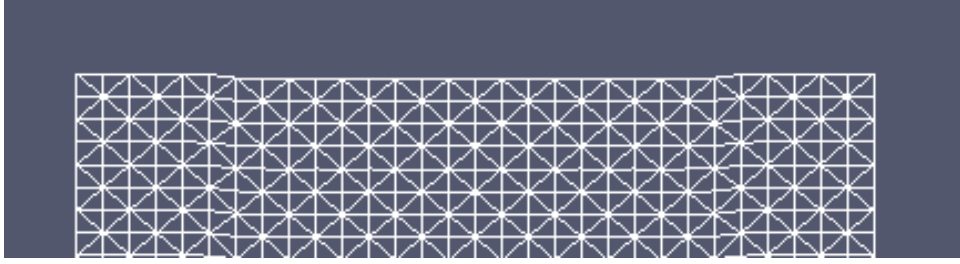
Figure 10: *A zoom of the upper region of the mesh at $t = 50\ My$. Notice that the region of source rock with positive initial kerogen concentration compacts more than the neighboring regions*

During the simulation, the burial of the domain caused by sedimentation makes the temperature increase until - after about 15 My - kerogen breakdown starts. In figure 11 we can observe the consumption of kerogen, which totally vanishes before half simulation.
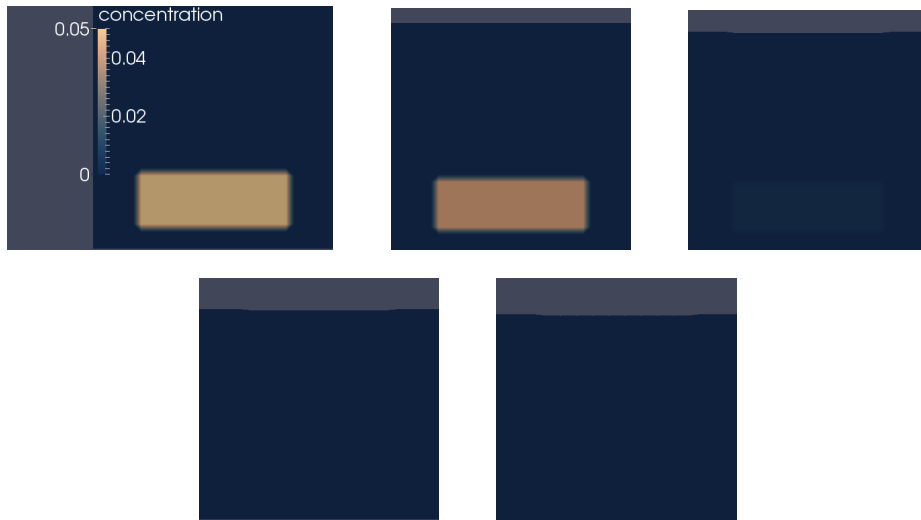

Figure 11: *Kerogen concentration at $t = 0$, $t = 17\ My$, $t = 27\ My$, $t = 40\ My$, and $t = 50\ My$.*

In figure 12 we can clearly see how the breakdown of kerogen causes an extra porosity, which will then be subject to compaction until, in the end, no trace of the initial kerogen is visible.

In figure 13, we compare the porosity obtained considering hydrocarbons generation (right hand side plot) and the porosity obtained with no kerogen consumption (left hand side plot) at the final instant of the simulation (i.e. 50 My). We can observe that in the region where kerogen was located the porosity, after 50 million years, is higher than in the surroundings.
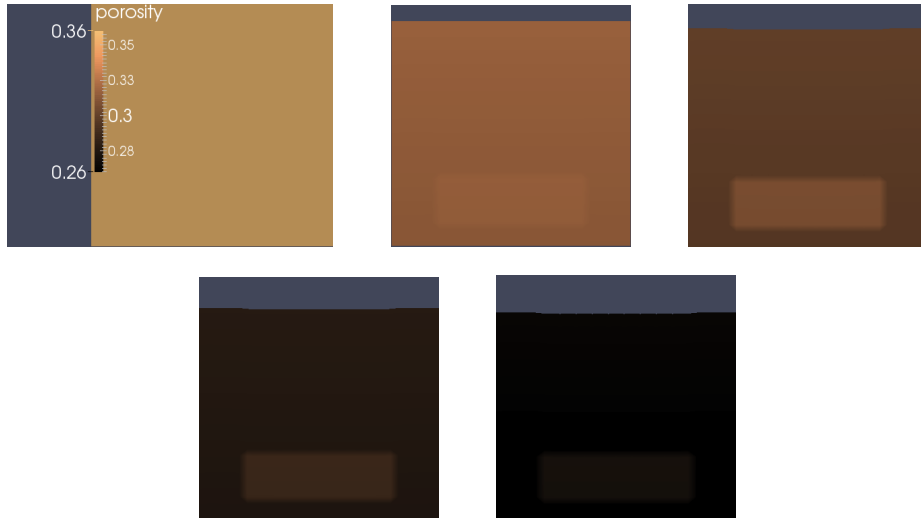
Figure 12: *Porosity at t = 0, t = 17 My, t = 27 My, t = 40 My, and t = 50 My.*

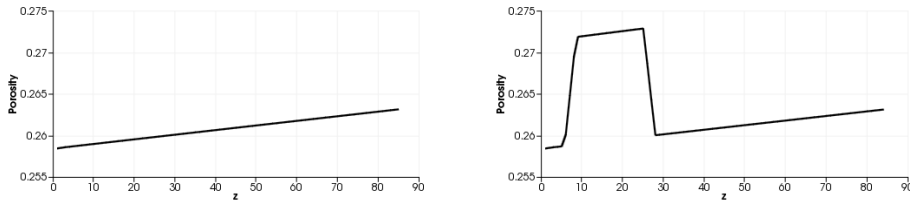Also, in the region with no kerogen, the porosity obtained with and without generation is the same.

Figure 13: *Plot of porosity versus z at t = 50 My, taken on a vertical line that halves the domain. The left side result is obtained with no kerogen degradation; the right hand side one is obtained with kerogen degradation.*

At the same time, as kerogen is consumed, oil saturation increases, until enough oil is present to be able to move in the source rock. In figure 15 an overpressure (i.e. the pressure in pores less hydrostatic pressure) is shown which does not allow the oil phase to reach the top of the source rock and forces it to move down (see figure 14).
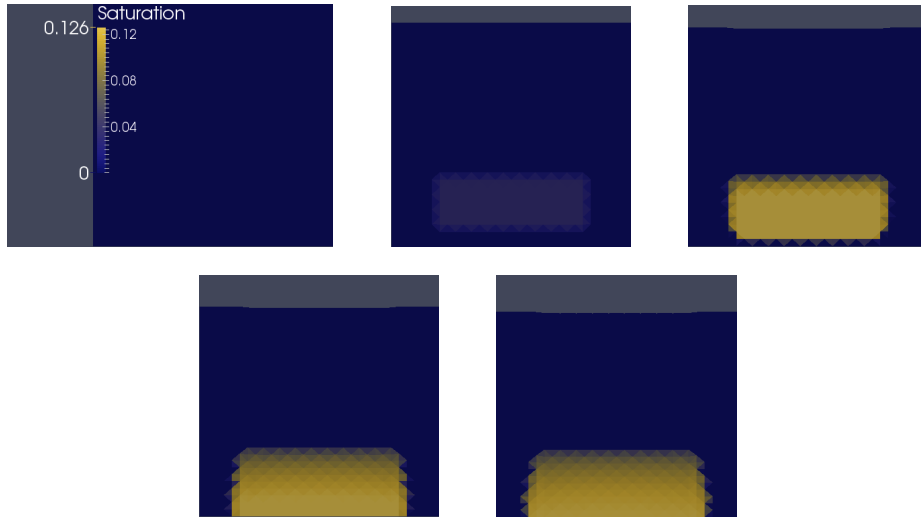
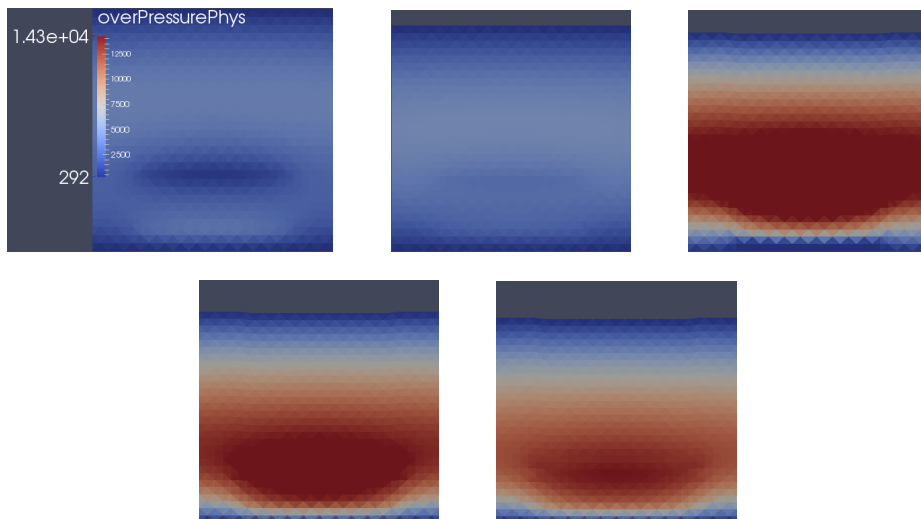Figure 14: *The oil saturation at $t = 0$, $t = 17$ My, $t = 27$ My, $t = 40$ My, and $t = 50$ My.*

Figure 15: *Overpressure at $t = 0$, $t = 17$ My, $t = 27$ My, $t = 40$ My, and $t = 50$ My.*

46

Comparison between two different pressure boundary conditions at the bottom

In order to understand if the overpressure observed in the previous test case (see figure 15) is physical or distorted by the pressure Dirichlet boundary condition at the bottom, we implemented a different boundary condition for a comparison. In particular we consider the case of hydrostatic pressure at the bottom and the case of a hydrostatic gradient imposed at the bottom, i.e. a Neumann condition for pressure requiring $\frac{\partial p}{\partial z} = -\rho_w g$ on Γ_{bot}.

In both the simulations, we consider an initial condition for kerogen consisting of a circle with $C_0 = 0.05$ in the lower part of the domain and we solve the full problem with the splitting strategy described in section 4.7 again. The only difference between the two simulations is the boundary condition for the global pressure at the bottom of the domain.

In figures 16 and 18 we show the evolution of the oil saturation in case of Dirichlet or Neumann boundary condition, respectively. No oil is present at the beginning of the simulation, because the breakdown of kerogen has not started yet. In figures 17 and 19 the evolution of the overpressure is shown. In case of Dirichlet boundary conditions for pressure it is clear that the overpressure (figure 17) does not allow the oil generated to move upwards, while in case of Neumann boundary conditions for pressure, the overpressure causes the oil to move upwards.
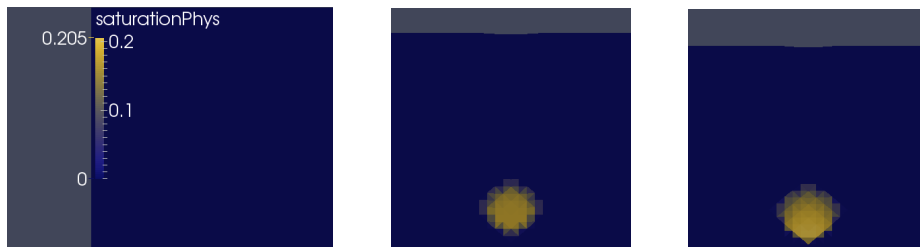

Figure 16: *Saturation at $t = 0$, $t = 30$ My, $t = 50$ My. With Dirichlet boundary conditions for pressure, the oil moves downwards.*

It is worth observing that the boundary condition for pressure at the bottom has a dramatic influence on oil migration. However, we point out that the correct boundary condition can be imposed only after a proper preliminary study of the geological properties of the source rock considered and of its surroundings and of the overlying and underlying layers.
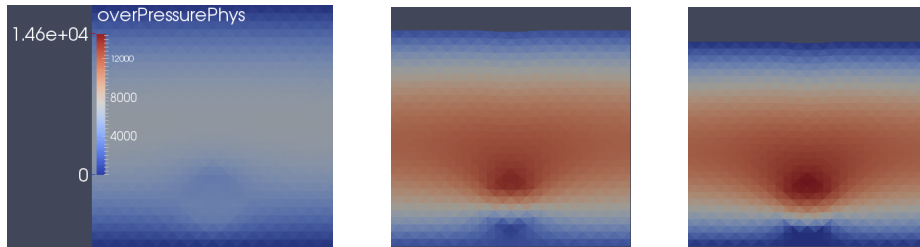
Figure 17: *Overpressure at $t = 0$, $t = 30$ My, $t = 50$ My, with Dirichlet boundary conditions for pressure.*
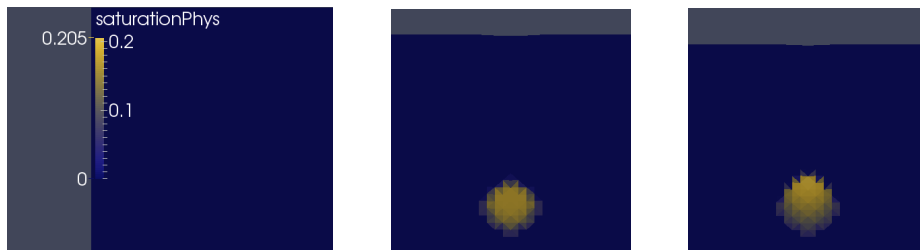

Figure 18: *Saturation at $t = 0$, $t = 30$ My, $t = 50$ My. With Neumann boundary conditions for pressure, the oil moves upwards.*
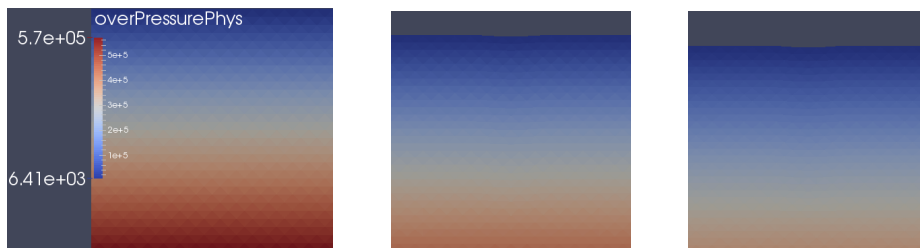

Figure 19: *Overpressure at $t = 0$, $t = 30$ My, $t = 50$ My, with Neumann boundary conditions for pressure.*

6 Conclusions and further developments

In this work, we have described and implemented a model for porosity evolution in source rock. The main purpose of this thesis was to gain insight into the complex interplay of mechanical and chemical processes and, as a first approximation, many simplifying assumptions were made. We have considered a chemical kinetics that involves only one type of kerogen and generates only oil, and we have neglected the effects of adsorption. The model proposed can be improved by considering different types of kerogen and products and by introducing the equations that govern the chemical reactions. Retention processes can also be included in the model. In this way, detailed simulations of generation and retention, coupled with a multi-phase and multi-component fluid flow, can be realized. Such an analysis allows to understand the composition of the hydrocarbons in the reservoirs, as well as the amount of the hydrocarbons retained in the source rock. This information has certainly deep economic implications.

Even though the model was simplified by the assumptions made, some numerical difficulties arose. In fact, instability problems were observed when solving the system for pressure and for the total velocity, when the time step was small and permeability reached low values. A simple fixed point strategy was enough in case of sufficiently high permeabilities ($k_0 \approx 10^{-6}$ Darcy), but too many fixed point iterations were necessary in case of lower permeabilities. In particular, we have observed in both the test cases of the Darcy problem and of the full problem, that the number of fixed point iterations necessary increased during the simulation. This happened because the progressive compaction due to the burial of the source rock caused the porosity and, consequently, the permeability to decrease. We are convinced that these instabilities can be strongly reduced by modifying, in the splitting strategy, the treatment of the porosity time derivative in the right hand side of equation (50), as suggested in the end of section 4.2.

The simulations conducted show that the overpressure in the domain is strongly influenced by the choice of the boundary conditions for pressure. In one case, by imposing at the bottom the hydrostatic pressure, the overpressure causes the newly generated oil to move downwards. In the other case, by imposing at the bottom the gradient of the hydrostatic pressure, oil moves upwards. Hence, a special attention should be payed to impose boundary conditions coherent with the geological setting considered. Moreover, since high pore fluid pressure can cause the rock to fracture, it would be interesting to expand the model by considering the possibility of rock fractures.

Although the model presented is general and was derived in d dimensions, where $d = 2$ or $d = 3$, the implementation of the numerical solver was in two dimensions. The most challenging further work is certainly the extension of the implementation to the three-dimensional case.

A Piola transformation of vectorial fields

In this appendix we explain how the equations (36) were obtained and what is the relationship between $\hat{\nabla} \cdot \hat{\mathbf{u}}$ and $\nabla \cdot \mathbf{u}$. In figure 20 we represent the two coordinate systems that we are working with. We denote with the hats the variables referred to the fixed domain and without the hats those referred to the physical one. Let $\boldsymbol{\varphi}_t : \hat{\Omega} \to \Omega(t)$ be the map from the fixed domain to the physical one at the instant $t \in (0, T]$. $\boldsymbol{\varphi}_t : \hat{\mathbf{x}} \mapsto \boldsymbol{\varphi}_t(\hat{\mathbf{x}}) = \mathbf{x}$.
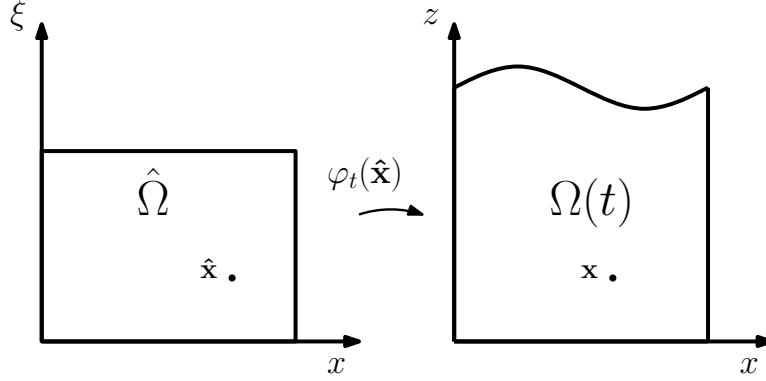

Figure 20: *The fixed domain and the physical one.*

Let $\hat{S} \in \partial\hat{\Omega}$ and $S_t = \boldsymbol{\varphi}_t(\hat{S})$. Let $\hat{\mathbf{n}}$ and $\mathbf{n}$ be the normal vectors, pointing outwards, to the boundaries $\hat{S}$ and S_t respectively. We consider a vectorial field $\mathbf{v}$ on $\Omega(t)$. The Piola transformation of $\mathbf{v}$ in $\hat{\Omega}$ is the vectorial field $\hat{\mathbf{v}}$ on $\hat{\Omega}$ such that

$$\int_{S_t} \mathbf{v} \cdot \mathbf{n} \, \mathrm{d}\Gamma = \int_{\hat{S}} \hat{\mathbf{v}} \cdot \hat{\mathbf{n}} \, \mathrm{d}\hat{\Gamma}.$$

With the notation of section 3.2.3, we define $\mathbf{J} := \nabla\boldsymbol{\varphi}_t$ and $J = \det \mathbf{J}$.

Proposition 5. *The Piola transformation of $\mathbf{v}$ is the vectorial field*

$$\hat{\mathbf{v}}(\hat{\mathbf{x}}, t) = J \, \mathbf{J}^{-1} \mathbf{v}(\boldsymbol{\varphi}_t(\hat{\mathbf{x}}), t).$$

Proof. It can be proved that for each triple of vectors $\mathbf{a}, \mathbf{b}, \mathbf{c}$

$$(\mathbf{Ja} \wedge \mathbf{Jb}) \cdot \mathbf{Jc} = J \, (\mathbf{a} \wedge \mathbf{b}) \cdot \mathbf{c}.$$

It follows that

$$\mathbf{J}^T (\mathbf{Ja} \wedge \mathbf{Jb}) \cdot \mathbf{c} = J \, (\mathbf{a} \wedge \mathbf{b}) \cdot \mathbf{c}.$$
$$\Rightarrow \mathbf{J}^T (\mathbf{Ja} \wedge \mathbf{Jb}) = J \, (\mathbf{a} \wedge \mathbf{b})$$

and, since $\mathbf{J}$ is invertible,

$$(\mathbf{Ja} \wedge \mathbf{Jb}) = J \, \mathbf{J}^{-T} (\mathbf{a} \wedge \mathbf{b}).$$

If $\hat{\mathbf{x}} : \mathcal{U} \to \hat{S}$, $\hat{\mathbf{x}} : (u^1, u^2) \mapsto \hat{\mathbf{x}}(u^1, u^2) \in \hat{S}$ is a parametrization of $\hat{S}$, $\boldsymbol{\varphi}_t \circ \hat{\mathbf{x}}$ is a parametrization of S_t. We can write

$$d\Gamma = \left| \frac{\partial \mathbf{x}}{\partial u^1} \wedge \frac{\partial \mathbf{x}}{\partial u^2} \right| du^1 \, du^2, \qquad d\hat{\Gamma} = \left| \frac{\partial \hat{\mathbf{x}}}{\partial u^1} \wedge \frac{\partial \hat{\mathbf{x}}}{\partial u^2} \right| du^1 \, du^2$$

and

$$\mathbf{n} = \frac{\frac{\partial \mathbf{x}}{\partial u^1} \wedge \frac{\partial \mathbf{x}}{\partial u^2}}{\left| \frac{\partial \mathbf{x}}{\partial u^1} \wedge \frac{\partial \mathbf{x}}{\partial u^2} \right|}, \qquad \hat{\mathbf{n}} = \frac{\frac{\partial \hat{\mathbf{x}}}{\partial u^1} \wedge \frac{\partial \hat{\mathbf{x}}}{\partial u^2}}{\left| \frac{\partial \hat{\mathbf{x}}}{\partial u^1} \wedge \frac{\partial \hat{\mathbf{x}}}{\partial u^2} \right|}.$$

Then, we have

$$\begin{aligned}
\int_{S_t} \mathbf{v} \cdot \mathbf{n} \, d\Gamma &= \int_{\mathcal{U}} \mathbf{v} \circ \boldsymbol{\varphi}_t \circ \hat{\mathbf{x}}(u^1, u^2) \cdot \mathbf{n}(u^1, u^2) \left| \frac{\partial \mathbf{x}}{\partial u^1} \wedge \frac{\partial \mathbf{x}}{\partial u^2} \right| du^1 \, du^2 \\
&= \int_{\mathcal{U}} \mathbf{v} \circ \boldsymbol{\varphi}_t \circ \hat{\mathbf{x}}(u^1, u^2) \cdot \left(\frac{\partial \mathbf{x}}{\partial u^1} \wedge \frac{\partial \mathbf{x}}{\partial u^2} \right) du^1 \, du^2 \\
&= \int_{\mathcal{U}} \mathbf{v} \circ \boldsymbol{\varphi}_t \circ \hat{\mathbf{x}}(u^1, u^2) \cdot \left(\mathbf{J} \frac{\partial \hat{\mathbf{x}}}{\partial u^1} \wedge \mathbf{J} \frac{\partial \hat{\mathbf{x}}}{\partial u^2} \right) du^1 \, du^2 \\
&= \int_{\mathcal{U}} \mathbf{v} \circ \boldsymbol{\varphi}_t \circ \hat{\mathbf{x}}(u^1, u^2) \cdot \mathbf{J}^{-T} \left(\frac{\partial \hat{\mathbf{x}}}{\partial u^1} \wedge \frac{\partial \hat{\mathbf{x}}}{\partial u^2} \right) J \, du^1 \, du^2 \\
&= \int_{\mathcal{U}} \mathbf{v} \circ \boldsymbol{\varphi}_t \circ \hat{\mathbf{x}}(u^1, u^2) \cdot \mathbf{J}^{-T} \, \hat{\mathbf{n}}(u^1, u^2) \left| \frac{\partial \hat{\mathbf{x}}}{\partial u^1} \wedge \frac{\partial \hat{\mathbf{x}}}{\partial u^2} \right| J \, du^1 \, du^2 \\
&= \int_{\hat{S}} J \, \mathbf{J}^{-1} \mathbf{v} \circ \boldsymbol{\varphi}_t \cdot \hat{\mathbf{n}} \, d\hat{\Gamma}
\end{aligned}$$

Since $\hat{S}$ is arbitrary, it follows that $\hat{\mathbf{v}} = J \, \mathbf{J}^{-1} \mathbf{v} \circ \boldsymbol{\varphi}_t$, which proves the thesis. $\qquad\square$

Corollary 1. *From the previous proposition it follows that*

$$\hat{\nabla} \cdot \hat{\mathbf{v}} = J \, \nabla \cdot \mathbf{v}.$$

Proof. If we take $S_t = \partial \Omega(t)$ and $\hat{S} = \hat{\Omega}$, we have

$$\int_{\Omega(t)} \nabla \cdot \mathbf{v} \, d\Omega = \int_{\partial \Omega(t)} \mathbf{v} \cdot \mathbf{n} \, d\Gamma = \int_{\partial \hat{\Omega}} \hat{\mathbf{v}} \cdot \hat{\mathbf{n}} \, d\hat{\Gamma} = \int_{\hat{\Omega}} \hat{\nabla} \cdot \hat{\mathbf{v}} \, d\hat{\Omega}.$$

By changing coordinates the first integral, since $\hat{\Omega}$ is arbitrary, we obtain that $J \, \nabla \cdot \mathbf{v} = \hat{\nabla} \cdot \hat{\mathbf{v}}$. $\qquad\square$

B The Raviart-Thomas elements

The Raviart-Thomas finite element space $\mathbf{RT}_0(\Omega, \mathcal{T}_h)$ is a finite element approximation of the space $H(\mathrm{div}; \Omega)$ defined by (52).

We consider a triangulation $\mathcal{T}_h$ of a simply-connected bounded domain $\Omega \subset \mathbb{R}^d$, with $d = 2$ or $d = 3$. For $D \subset \Omega$, we refer to $\mathcal{N}_h$, $\mathcal{E}_h$, and $\mathcal{F}_h$ as the sets of vertices, edges, and faces in D. We denote by $P_k(D)$ and $\tilde{P}_k(D)$, $k \in \mathbb{N}_0$, the sets of polynomials of degree $\leq k$ and the set of homogeneous polynomials of degree k on D.

For $K \in \mathcal{T}_h$ and $k \in \mathbb{N}_0$, we set

$$R_k(\partial K) := \{\varphi \in L^2(\partial K) : \{\varphi|_e \in P_k(e), e \in \mathcal{E}_h(K)\} \text{ if } d = 2,$$

$$R_k(\partial K) := \{\varphi \in L^2(\partial K) : \{\varphi|_f \in P_k(f), f \in \mathcal{F}_h(K)\} \text{ if } d = 3.$$

Let k be a d-symplex. The Raviart-Thomas element $\mathbf{RT}_k(K)$, $k \in \mathbb{N}_0$ is defined by

$$\mathbf{RT}_k(K) = P_k(K)^d + \mathbf{x}P_k(K).$$

Proposition 6. *If $\mathbf{q} \in \mathbf{RT}_k(K)$, then*

$$\nabla \cdot \mathbf{q} \in P_k(K),$$

$$\mathbf{n} \cdot \mathbf{q}|_{\partial K} \in R_k(\partial K).$$

Moreover,

$$dim\ \mathbf{RT}_k(K) = \begin{cases} (k+1)(k+3) & \text{if } d = 2 \\ \dfrac{1}{2}(k+1)(k+2)(k+4) & \text{if } d = 2 \end{cases}$$

In case $d = 2$, the degrees of freedom on each element K for the cases $k = 0$ and $k = 1$ are those shown in figure 21.
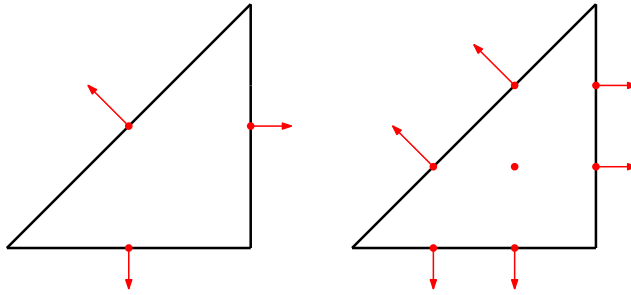

Figure 21: *Degrees of freedom of $\mathbf{RT}_k(K)$ with $k = 0$ and $k = 1$, $d = 2$.*

If $k = 0$ and $d = 2$, that is the case of our application, the basis functions of the Raviart-Thomas finite elements are

$$\tau_i^K = \frac{\mathbf{x} - \mathbf{x}_i}{2|K|} \qquad \forall \mathbf{x} \in K$$

We can now define the Raviart-Thomas finite element space $\mathbf{RT}_0(\Omega, \mathcal{T}_h)$ as

$$\mathbf{RT}_k(\Omega, \mathcal{T}_h) := \{\mathbf{q} \in L^2(\Omega)^d : \mathbf{q}|_K \in \mathbf{RT}_k(K), K \in \mathcal{T}_h\}$$

$\mathbf{RT}_k(\Omega, \mathcal{T}_h)$ is a finite dimensional subspace of $H(\mathrm{div}; \Omega)$.

C   Adsorption Isotherms

Recent years studies have classified the retention processes into three different types: the absorption of petroleum compounds in kerogen, the adsorption on vitrinite surface and the adsorption in mineral nanopores. The main idea of absorption in kerogen is that kerogen is a macromolecule that behaves like a polymer and is thus able to dissolve other species in its molecular structure. Instead, adsorption is a surface phenomenon that occurs when a gas or liquid solute accumulates on the surface of a solid forming a molecular film.

The software used in this appendix for the simulation of generation and primary migration is Pmod+, owned by Eni S.p.A. . The approach used in Pmod+ to describe the retention processes consists of three stacked filters, one for each different type of retention, characterized by a maximum retention threshold for each hydrocarbon species. If the amount generated by chemical reactions is below a retention threshold it is fully retained by the filter, otherwise a fraction is retained and the remaining part is expelled from the source rock. It should be pointed out that the retention thresholds depend strongly on the molecular properties of the hydrocarbons, therefore the filters have different effects on the various species: those that are more likely to be retained keep undergoing cracking reactions and transform into lighter hydrocarbons, resulting in a change in the chemical composition of petroleum and gas. The thresholds are defined by experimental laws and depend, in general, they depend on time and on the concentration of the species.

In this appendix, we simulate the generation and expulsion of hydrocarbons in a source rock with particular focus on adsorption in mineral nanopores. Adsorption is usually described through isotherms that represent the amount of adsorbed fluid on the adsorbent as a function of its concentration (or partial pressure, in case more than one fluid is considered) at a constant temperature. The most common adsorption models proposed in literature are Langmuir, Freundlich, and Romero-Sarmiento isotherms. The first model can be derived with rigorous chemical and statistical arguments. The second model is an empirical equation and is the only model originally implemented in Pmod+. Finally, the third model is a generalization of Langmuir isotherm. After implementing in Pmod+ the Langmuir and the R-S isotherms, with the possibility of selecting the desired model with the new flag ADSHALE, the results obtained with different adsorption models are compared.

Langmuir Isotherm

The equation of Langmuir isotherm can be derived straightforward from the following assumptions:

- There is a dynamic equilibrium between the adsorbed molecules and the free ones.

- The solute molecules can be adsorbed in a fixed number of sites, which are equal in size and shape. Each site can hold a maximum of one molecule.

- The adsorption involves the attachment of only one layer of molecules to the surface.

- There is no interaction between the molecules of the adsorbate.

Let A and S be the adsorbate and the adsorbant respectively. More precisely A denotes the unadsorbed molecules and B the vacant sites of the surface. The chemical reaction that represents the monolayer adsorption can be written as follows:
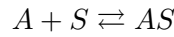
$$A + S \rightleftarrows AS$$

where AS represents a solute molecule bound to a surface site on S, that is an adsorbed molecule.

The equilibrium constant for this reaction is

$$K_L = \frac{[AS]}{[A][S]}$$

where $[A]$ denotes the concentration of the adsorbate and $[S]$ and $[AS]$ are a sort of concentration expressed in terms of mol/cm^2. Let θ be the fraction of the occupied sites and $1 - \theta$ the fraction of the vacant ones. We expect $[AS]$ to be proportional to θ and $[S]$ to $1 - \theta$ so that

$$\frac{[AS]}{[S]} = \frac{\theta}{1 - \theta}$$

Denoting with c the concentration of the adsorbate, one has

$$K_L = \frac{\theta}{c(1 - \theta)}$$

that is

$$\theta = \frac{K_L c}{1 + K_L c}$$

In terms of adsorbate moles, we can express θ as $\frac{z}{z_{max}}$, where z is the amount adsorbed and z_{max} is the maximum amount that can be stored due to adsorption. Thus,

$$z = z_{max} \frac{K_L c}{1 + K_L c} \tag{58}$$

that is the equation of Langmuir Isotherm. K_L $[-]$ and z_{max} $[kg/kg_{rock}]$ are empirically determined and do not depend on temperature. In case more than one species are involved, we should replace in (58) the concentration c with the relative concentrations r_i. z_{max} and K_L may be significantly different for different species.

Freundlich Isotherm

The equation of Freundlich isotherm is:

$$z = K_F \ c^{1/n} \qquad n > 1 \tag{59}$$

where K_F $[kg/kg_{rock}]$ and n $[-]$ are experimental constants. Freundlich isotherm is an empirical adsorption model, that can be seen in certain conditions as an approximation of the previous model. In (58), if $K_L c << 1$ then $z \simeq z_{max} K_L c$, while, if $K_L c >> 1$ then $z \simeq z_{max}$. In the first case, (59) well approximate (58) if $n = 1$, while in the latter case it should be $n \to \infty$. Despite this affinity, Langmuir and Freundlich models are deeply different. Contrary to the Langmuir model, where the isotherm reaches an asymptote when the system is completely saturate, in this model there is not a maximum adsorption capacity. For this reason, Freundlich isotherm is preferable when we want to model multilayer adsorption.

Romero-Sarmiento Isotherm

In [6], Zhang et al. proved that methane adsorption in organic rich shales is greatly affected by TOC content. In particular, CH4 adsorption capacity was shown to increase with increasing TOC concentration in kerogen. A variation of Langmuir classic model that represents the correlation of the adsorbed volume with the TOC in place is proposed by Romero-Sarmiento in [5]. This model also accounts for a possible dependence on the temperature of the adsorbed amount. In fact, Romero-Sarmiento isotherm is a variation of Langmuir isotherm:

$$z = y_{max} \ TOC_{sm} \ \frac{K_L(T) \ P}{1 + K_L(T) \ P} \tag{60}$$

where

$$K_L(T) = C \ e^{\frac{A}{T}+B}.$$

T $[K]$ is the absolute temperature, P $[Pa]$ is the pressure. A $[K]$, B $[-]$ and C $[1/Pa]$ are three parameters derived experimentally from the adsorption isotherms. y_{max} $[kg/kg_C]$ is the carbon maximum adsorption capacity and is related to the number of adsorption sites for a given mass of carbon. Finally, TOC_{sm} $[kg_C/kg_{rock}]$ is the amount of TOC still present in rock in the form of solid matter, and can be obtained as

$$TOC_{sm} = TOC_{ker} + TOC_{res}$$

where $TOC_{ker} = TOC_0(1 - TR)$ is the TOC in the immature kerogen and TOC_{res} is the residual solid TOC resulting from the solid products of the kerogen transformation.

Implemented Models

The isotherms mentioned above are implemented in terms of the relative concentrations of the various species $i = 1, ..., M$. Depending on the value of the new variable ADSHALE in the .pri input file, Pmod+ will use a different adsorption model.

Model 0

For ADSHALE $= 0$, Pmod+ will use the original model, a variant of Freundlich isotherm proposed by Ritter and discussed in [18]. For the i-th species, the adsorbed amount is:

$$z_i = W_i r_i^{f_i(\mathbf{r})}$$

$$f_i(\mathbf{r}) = \frac{\left(\sum_j \delta_j r_j - \delta_i\right)^{SI}}{UD}$$

Note that W_i $[kg_i/kg_{rock}]$ and f_i $[-]$ are different for each species, while SI and UD have fixed values: $SI = 0.8$ and $UD = 3.0$. δ_j are the Hildebrand solubility parameters as described in [18].

Model 1

For ADSHALE $= 1$ a Langmuir isotherm is used. Because the experimental isotherms are often described as

$$V_i = V_{L,i} \frac{P_i}{P_{L,i} + P_i}$$

where $V_{L,i}$ $[scf_i/ton_{rock}]$ and $P_{L,i}$ $[Pa]$, these parameters will be required in the .pri input file. $V_{L,i}$ will be then converted in scm_i/kg_{rock} and the adsorbed amount $z_i = V_i \ \rho_i$ $[kg_i/kg_{rock}]$ is given by:

$$z_i = \rho_i \ V_{L,i} \frac{P \ r_i}{P_{L,i} + P \ r_i} = \rho_i \ V_{L,i} \frac{r_i}{\frac{P_{L,i}}{P} + r_i}.$$

Note that scm are m^3 at standard conditions (i.e. $T = 15.6$ °C and $P = 1 \ atm$). For this reason, ρ_i $[kg_i/m^3]$ must be the density of the i-th species at standard conditions and not the effective density in the rock.

Model 2

For ADSHALE = 2 a Freundlich isotherm is implemented. The input values are $V_{F,i}$ $[scf_i/ton_{rock}]$ and $n_{F,i}$ $[-]$. Similarly to the previous case $V_{L,i}$ is converted into scm_i/kg_{rock} and z_i is

$$z_i = \rho_i \ V_{F,i} \ r_i^{1/n_{F,i}}$$

Since no experimental calibration has been done for this model, numerical results for this case will not be analysed.

Model 3

For ADSHALE = 3, Romero Sarmiento isotherm is used, exactly as described in (60). Thus,

$$z_i = y_{max,i} \ TOC_{sm} \ \frac{K_L(T) \ P}{1 + K_L(T) \ P}$$

In [5] the values of the parameters proposed are the following: $A = 2628 \ K$, $B = -9.754$, $C = 10^{-6} \ 1/Pa$, while $y_{max,i} = 0.0215 \ kg_i/kg_C$ for methane adsorption.

Results

In this section, the numerical results obtained for four different adsorption isotherms are compared: the originally implemented Ritter model, two Langmuir models with two different choices of the parameters and Romero Sarmiento (RS). Langmuir 1 is obtained with $V_{L,i} = 76.25 \ scf_i/ton_{rock}$ and $P_{L,i} = 21.31 MPa$ and Langmuir 2 with $V_{L,i} = 55.37 \ scf_i/ton_{rock}$ and $P_{L,i} = 22.50 MPa$. These couples of values are taken from the CoreLab data available for the adsorption of methane in the Barnett Shale in Shifflett well and for depths comparable to that of the geological model used for these simulations. Since no data regarding the adsorption isotherms of the other fluid species were available, the same parameters were used for each component. A sketch of the two Langmuirs is presented in figure 22.

A set-up that well highlights the differences between the adsorption isotherms discussed was used. The only kind of retention in rock considered was adsorption in shale (i.e. only the third filter of those implemented in Pmod+ was activated) and an open system with full expulsion of all the free species was studied (i.e. the flag ISYS was set to 5). Observe that, if all the free species in rock are expelled, the remaining in rock amount coincides with the adsorbed amount. The chemical kinetic consisted of the simplified scheme:

$$KER1 \ \rightarrow OLIO, \ CHX, \ KER2$$
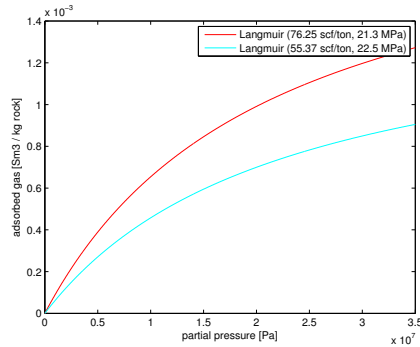$$OLIO \ \rightarrow CHX, \ CH4, \ KER2.$$
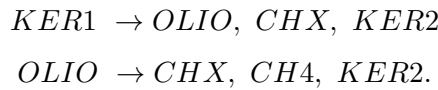
Figure 22: Isotherms: red = Langmuir 1, pale blue = Langmuir 2.

As expected, the remaining gas in the source rock is deeply influenced by the choice of the adsorption model, as shown in figure 23. Concerning the two Langmuirs, the higher one (i.e. in our case Langmuir 1) causes a higher retention for both CH4 and CHX. With RS model for CH4 adsorption, one can observe that remaining in rock CH4 is much lower than the quantity predicted by the other models. This is due to the fact that the adsorption amount in this model is inversely proportional to the absolute temperature and that the secondary cracking from whom methane is generated occurs at high temperatures. Thus, most of the methane is expelled immediately after generation.

Because the remaining methane is significantly lower when RS adsorption model is used, the total gas remaining in rock (i.e. the adsorbed quantity, since full expulsion means there is no free gas in rock) with model RS is much lower compared to the other cases, as one can see in figure 24.

In figure 23, one can observe that the remaining amount of CH4 reaches a constant value once all the CH4 is generated. On the other hand, the remaining amount of CHX seems to reach a constant value after primary cracking is completed, and starts growing again when secondary cracking begins. In fact, CHX is both a primary and a secondary product in this chemical kinetic. RS isotherm is the only one that does not show this behaviour. The reason for this is explained below.

As expected, the oil generation (figure 25) does not depend on the adsorption model. In fact, in this kinetic oil is only a first generation product. Concerning the oil remaining, the curves relative to the two Langmuir models overlap, while RS prediction is far lower than the others. This means that, in the latter case, the amount of the products obtained with the secondary cracking will be lower. This explains why in the RS case the remaining CHX presents only one flat region, once most of the CHX is generated.

Pure Langmuir gas expulsion is quite similar for the two choices of the parameters for both CH4 and CHX expulsion, as shown in figure 26.
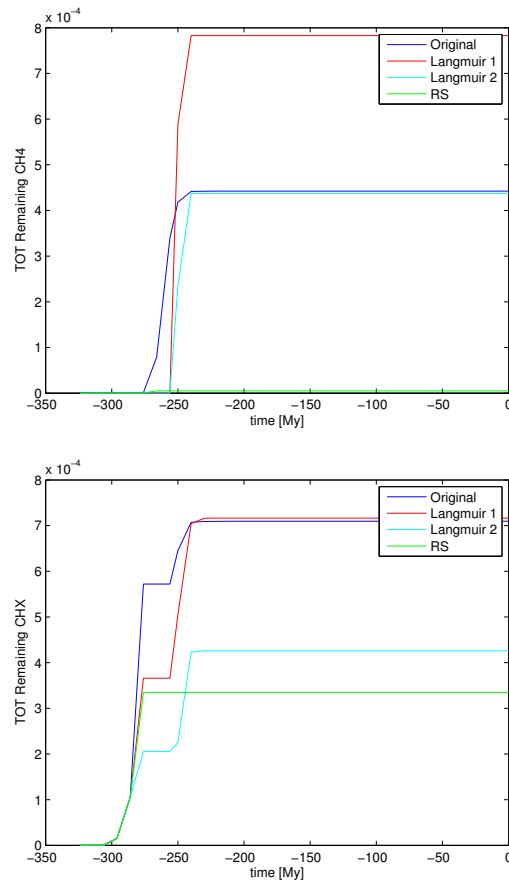
Figure 23: Remaining gas $[kg_i/kg_{rock}]$.

Notice that the variables referred to CH4 are more sensible to the choice of the adsorption model than those referred to CHX. This is due to the extremely simplified kinetic scheme used, where CHX can be generated by both the first and the second kerogen cracking, while CH4 is only a second generation product. Of course, the more oil is retained and the more CH4 is generated and expelled. This is clearly shown in figures 27 and 26.

In figures 28 and 29 are represented the generated, retained, and expelled amounts of CH4 and CHX for each adsorption model.
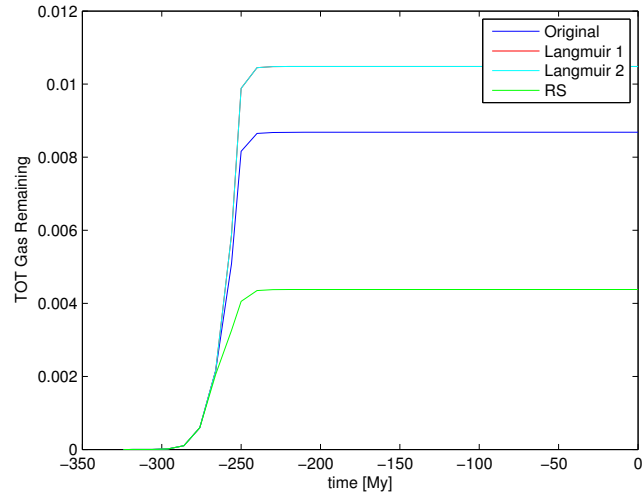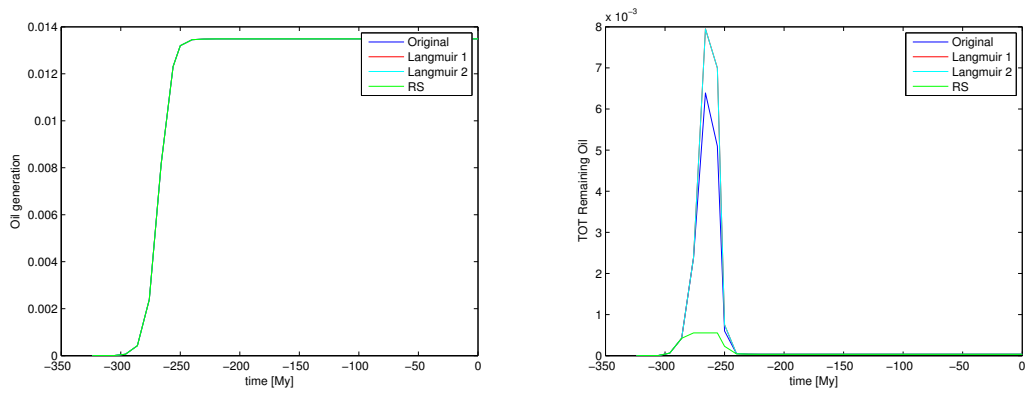
Figure 24: Remaining gas $[kg_i/kg_{rock}]$.

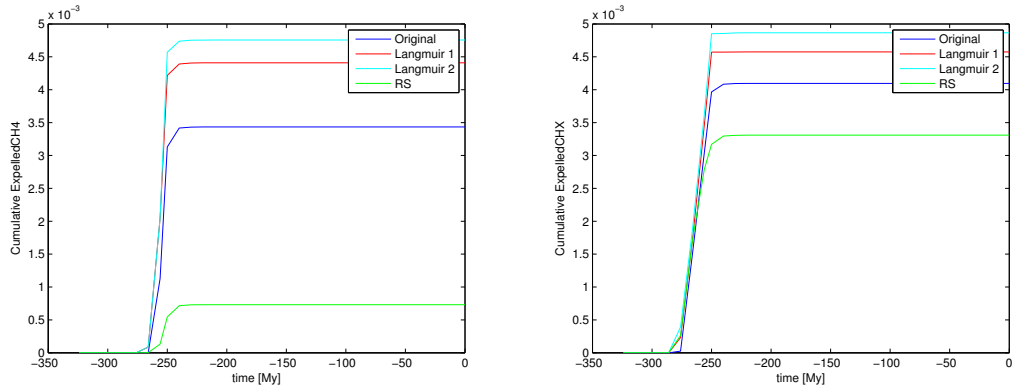Figure 25: Oil generation and oil remaining $[kg_i/kg_{rock}]$.
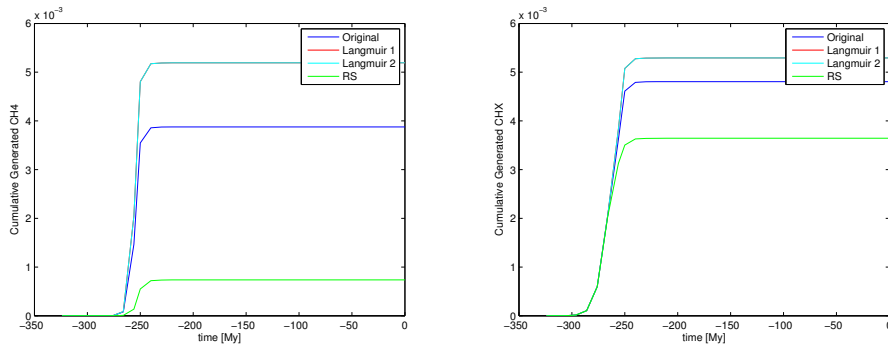
Figure 26: Expelled gas $[kg_i/kg_{rock}]$.
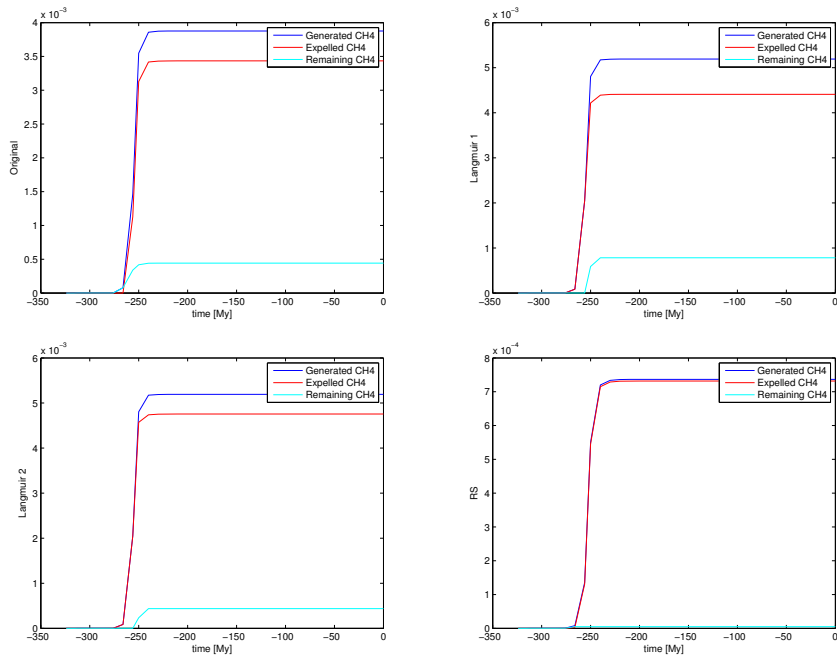

Figure 27: Generated gas $[kg_i/kg_{rock}]$.

Figure 28: CH4 generation, expulsion, retention $[kg_i/kg_{rock}]$.

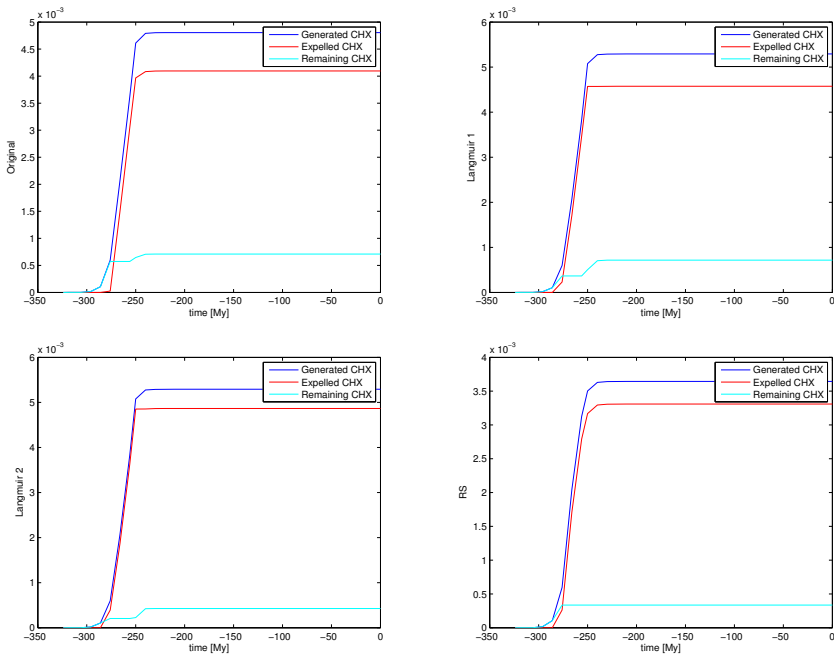Figure 29: CHX generation, expulsion, retention $[kg_i/kg_{rock}]$.

References

[1] *Hydrocarbons Encyclopedia.* Treccani, 2005.

[2] Guy Chavent and Gérôme Jaffré. *Mathematical models and finite elements for reservoir simulation.* Elsevier Science Publishers B.V., 1986.

[3] Zhangxin Chen. Expanded mixed finite element methods for linear second-order elliptic problems. *M2AN*, 4:479–499, 1998.

[4] Zhangxin Chen, Richard E. Ewing, Hao Lu, Stephen L. Lyons, Serguei Maliassov, Micheal B. Ray, and Tong Sun. Integrated two-dimensional modeling of fluid flow and compaction in a sedimentary basin. *Computational Geosciences*, 6:545–564, 2002.

[5] M. F. Romero-Sarmiento et al. Quantitative evaluation of toc, organic porosity and gas retention distribution in a gas shale play using petroleum system modeling: Application to the mississippian barnett shale. *Elsevier Marine and Petroleum Geology*, 45:315–330, 2013.

[6] T. Zhang et al. Effect of organic-matter type and thermal maturity on methane adsorption in shale-gas systems. *Elsevier Organic Geochemistry*, 47:120–131, 2012.

[7] Andrew C. Fowler and Xin-She Yang. Fast and slow compaction in sedimentary basins. *SIAM Journal on Applied Mathematics*, 59:365–385, 1998.

[8] Andrew C. Fowler and Xin-She Yang. Pressure solution and viscous compaction in sedimentary basins. *Journal of geophysical research*, 104:12989–12997, 1999.

[9] Alessio Fumagalli. *Numerical modelling of flows in fractured porous media by the XFEM method.* PhD thesis, Politecnico di Milano, 2012.

[10] Marte Gutierrez and Magnus Wangen. Modeling of compaction and overpressuring in sedimentary basins. *Elsevier Marine and Petroleum Geology*, 22:351–363, 2005.

[11] Thomas Hantschel and Armin I. Kauerauf. *Fundamentals of Basin and Petroleum Systems Modeling.* Springer Berlin / Heidelberg, 2009.

[12] X Luo, G Vasseur, and A Pouya. Elastoplastic deformation of porous media applied to the modelling of compaction at basin scale. *Elsevier Marine and Petroleum Geology*, 15:145–162, 1998.

[13] J. Nitsche. Über ein Variationsprinzip zur Lösung von Dirichlet-Problemen bei Verwendung von Teilräumen, die keinen Randbedingungen unterworfen sind. *Abhandlungen aus dem Mathematischen Seminar der Universität Hamburg*, 36:9–15, 1971.

[14] F. O. Okeola and E. O. Odebunmi. Comparison of freundlich and langmuir isotherms for adsorption of methylene blue by agrowaste derived activated carbon. *Advances in Environmental Biology*, 4:329–335, 2010.

[15] Xiongqi Pang, Zhenxue Jiang, Shengjie Zuo, and Ian Lerche. Dynamics of hydrocarbon expulsion from shale source rocks. *Energy Exploration & Exploitation*, 23:333–355, 2005.

[16] Ulrich Ritter. Solubility of petroleums compounds in kerogen: implications for petroleum expulsion. *Elsevier Organic Geochemistry*, 34:319–326, 2003.

[17] Ulrich Ritter and Arnt Grover. Adsorption of petroleum compounds in vitrinite: implications for petroleum expulsion from coal. *International Journal of Coal Geology*, 63:183–191, 2005.

[18] Anna Scotti. *A numerical model for generation, retention and expulsion of hydrocarbons from source rock*. PhD thesis, Politecnico di Milano, 2010.

[19] M. Vandenbroucke and C. Largeau. Kerogen origin, evolution and structure. *Elsevier Organic Chemistry*, 38:719–833, 2007.

[20] Magnus Wangen. Pressure and temperature evolution in sedimentary basins. *Geophysical Journal International*, 110:601–613, 1992.

[21] Magnus Wangen. Vertical migration of hydrocarbons modelled with fractional flow theory. *Geophysical Journal International*, 115:109–131, 1993.

[22] Magnus Wangen. Two-phase oil migration in compacting sedimentary basins modelled by the finite element method. *International Journal for Numerical and Analytical Methods in Geomechanics*, 21:91–120, 1997.

[23] Magnus Wangen. Modeling porosity evolution and cementation of sandstones. *Marine and petroleum geology*, 15:453—-465, 1998.

[24] Magnus Wangen. A quantitative comparison of some mechanisms generating overpressure in sedimentary basins. *Elsevier Tectonophysics*, 334:211–234, 2001.

[25] Magnus Wangen. *Physical principles of sedimentary basin analysis*. Cambridge University Press, 2010.

[26] Xin-She Yang. *Mathematical modelling of compaction and diagenesis in sedimentary basins*. PhD thesis, University of Oxford, 1997.

[27] Xin-She Yang. Nonlinear viscoelastic compaction in sedimentary basins. *Nonlinear Processes in Geophysics*, 7:1–7, 2000.

[28] Xin-She Yang. A unified approach to mechanical compaction, pressure solution, mineral reactions and the temperature distribution in hydrocarbon basins. *Elsevier Tectonophysics*, 330:141–151, 2001.

[29] Ivan Yotov. A mixed finite element discretization on non-matching multiblock grids for a degenerate parabolic equation arising in porous media flow. *East-West Journal of Numerical Mathematics*, 1:1–21, 1997.